AD-A138 332 A STUDY OF OPTICAL AMPLIFICATION IN A DOUBLE HETEROSTRUCTURE GAAS DEVIEE..(U) AEROSPACE CORP EL SEGUNDO CA ELECTRONICS RESEARCH LAB M T TAVIS

1/1

UNCLASSIFIED 15 DEC 83 TR-0084(4925-03)-1 SD-TR-83-75 F/G 20/5 NL

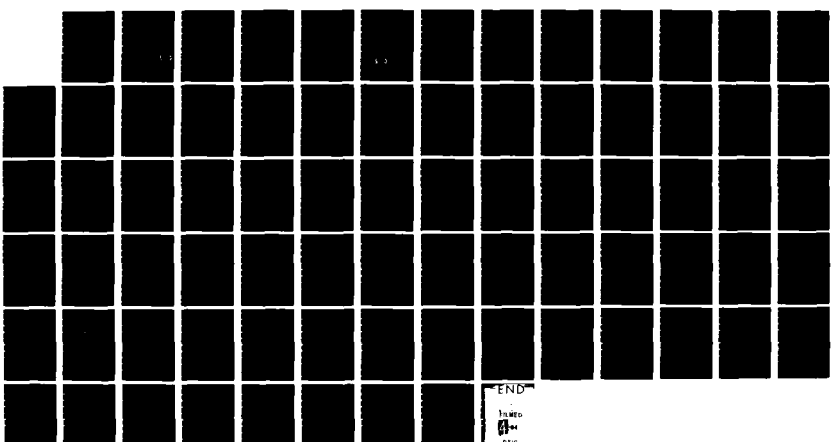

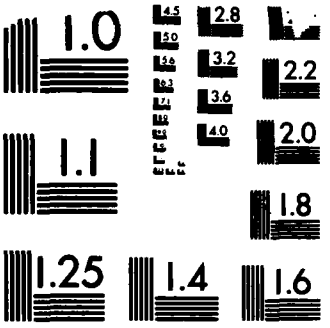

MICROCOPY RESOLUTION TEST CHART
NATIONAL BUREAU OF STANDARDS-1963-A

ORT SD-TR-83-75

A Study of Optical Amplification in a Double Heterostructure GaAs Device Using the Density Matrix Approach

M. T. TAVIS
Electronics Research Laboratory
Laboratory Operations
The Aerospace Corporation
El Segundo, Calif. 90245

15 December 1983

Prepared for
SPACE DIVISION
AIR FORCE SYSTEMS COMMAND
Los Angeles Air Force Station
P.O. Box 92960, Worldway Postal Center
Los Angeles, Calif. 90009

This report was submitted by The Aerospace Corporation, El Segundo, CA 90245, under Contract No. F04701-83-C-0084 with the Space Division, Deputy for Technology, P.O. Box 92960, Worldway Postal Center, Los Angeles, CA 90009. It was reviewed and approved for The Aerospace Corporation by D. H. Phillips, Director, Electronics Research Laboratory. Second Lt. Russell R. Herndon, SD/AFSTC (WCO) was the project officer for the Mission Oriented Investigation and Experimentation (MOIE) Program.

This report has been reviewed by the Public Affairs Office (PAS) and is releasable to the National Technical Information Service (NTIS). At NTIS, it will be available to the general public, including foreign nationals.

This technical report has been reviewed and is approved for publication. Publication of this report does not constitute Air Force approval of the report's findings or conclusions. It is published only for the exchange and stimulation of ideas.

Russell R. Herndon, 2nd Lt, USAF
Project Officer

Joseph Hess, GM-15, Director
West Coast Office, AF Space
Technology Center

UNCLASSIFIED

SECURITY CLASSIFICATION OF THIS PAGE *(When Data Entered)*

REPORT DOCUMENTATION PAGE		READ INSTRUCTIONS BEFORE COMPLETING FORM
1. REPORT NUMBER SD-TR-83-75	2. GOVT ACCESSION NO. AD-A138	3. RECIPIENT'S CATALOG NUMBER 982
4. TITLE *(and Subtitle)* A STUDY OF OPTICAL AMPLIFICATION IN A DOUBLE HETEROSTRUCTURE GaAs DEVICE USING THE DENSITY MATRIX APPROACH		5. TYPE OF REPORT & PERIOD COVERED 6. PERFORMING ORG. REPORT NUMBER TR-0084(4925-03)-1
7. AUTHOR(s) Michael T. Tavis		8. CONTRACT OR GRANT NUMBER(s) F04701-83-C-0084
9. PERFORMING ORGANIZATION NAME AND ADDRESS The Aerospace Corporation El Segundo, Calif. 90245		10. PROGRAM ELEMENT, PROJECT, TASK AREA & WORK UNIT NUMBERS
11. CONTROLLING OFFICE NAME AND ADDRESS Space Division Los Angeles Air Force Station Los Angeles, Calif. 90009		12. REPORT DATE 15 December 1983 13. NUMBER OF PAGES 72
14. MONITORING AGENCY NAME & ADDRESS*(if different from Controlling Office)*		15. SECURITY CLASS. *(of this report)* Unclassified 15a. DECLASSIFICATION/DOWNGRADING SCHEDULE

16. DISTRIBUTION STATEMENT *(of this Report)*

Approved for Public Release; Distribution Unlimited.

17. DISTRIBUTION STATEMENT *(of the abstract entered in Block 20, if different from Report)*

18. SUPPLEMENTARY NOTES

19. KEY WORDS *(Continue on reverse side if necessary and identify by block number)*

AlGaAs Traveling Wave Light Amplifiers
Density Matrix Formulation of Laser Amplifiers
Intraband Relaxation Processes in GaAs Lasers
Multipulse Operation of AlGaAs Traveling Wave Light Lasers
Solid-State Theory

20. ABSTRACT *(Continue on reverse side if necessary and identify by block number)*

A theoretical investigation of traveling wave light amplification in a GaAs double heterostructure device is presented in this report. The analysis is self-consistent and semiclassical, and uses a density matrix formulation. Phenomenological constants are included to account for intraband relaxation processes, pumping, and spontaneous emission. The analysis is significantly different from previous rate equation approaches in that saturation effects

DD FORM 1473 (FACSIMILE)

UNCLASSIFIED

SECURITY CLASSIFICATION OF THIS PAGE *(When Data Entered)*

19. KEY WORDS (Continued)

20. ABSTRACT (Continued)

are inherent in the results and phase information, important for coherent applications, is retained. Results presented for steady state and pulsed operation include gain, pulse compression, multi-pulse effects, and the phase variation that occurs over the pulse time.

PREFACE

The author is indebted to Dr. John Tucker and Dr. John Hurrell for extensive technical discussions concerning this subject. I also wish to thank Dr. Wayne R. Fenner and Dr. Elsa M. Garmire for their active support and many editorial suggestions, without which this manuscript would not have been completed.

CONTENTS

PREFACE 1

I. INTRODUCTION 9

A. Background 9

B. Summary of Results 11

C. Theoretical Assumptions 11

II. THEORY 15

A. General Equations 15

B. Steady State 20

C. Pulsed Operation 23

III. NUMERICAL RESULTS AND DISCUSSION 25

A. Steady State 25

B. Pulsed Operation 37

C. Multi-Pulse Effects 41

IV. CONCLUSIONS 47

REFERENCES 49

APPENDIX: NONREGENERATIVE OPTICAL AMPLIFICATION IN MONOLITHIC GaAs 53

FIGURES

1. Steady-state intensity response of a GaAs amplifier..... 29

2. Steady-state phase response of a GaAs amplifier..... 30

3. Steady-state intensity response of a GaAs amplifier..... 33

4. Steady-state phase response of a GaAs amplifier..... 34

5. GaAs amplifier intensity response to a single input modified sinusoidal pulse for various device lengths..... 38

6. GaAs amplifier phase response to a single input modified sinusoidal pulse for various device lengths..... 40

7. GaAs amplifier intensity response to a set of six input pulses..... 42

8. GaAs amplifier phase response to a set of six input pulses..... 43

TABLES

I. Assumed Device Parameters..... 26

II. Optical Input Parameters and Calculated Results..... 27

III. Alternate Optical Input Parameters and Calculated Small Signal Gain..... 35

I. INTRODUCTION

A. Background

A theoretical investigation of the phase and amplitude behavior of light pulses amplified in a GaAs double heterostructure device including the effect of intraband relaxation processes applied to the individual momentum states is presented. Fast intraband processes were considered in early work concerning the quantum mechanical treatment of fluctuations, relaxation, and noise in semiconductor lasers [1,2]. These processes were assumed to be so fast compared to all times of interest that each electron and corresponding hole was considered to be in thermal equilibrium with all the other electrons and holes. In this report we do not require that processes be fast, and we calculate the transition for each state separately. These processes were also considered in a nonlinear treatment for laser diodes [3], modeled in terms of relaxation times required for electrons and holes as an entirety to come to quasi equilibrium. The concept of very fast intraband relaxation processes resulted in the use of a single two-level system representing all the electrons and holes. With this concept intraband relaxation processes could be ignored and a single rate equation written for the population inversion. This equation, plus a rate equation for photon number density and the Fabry-Perot (F-P) oscillator condition for simple resonators, permitted analysis of the semiconductor laser applied to communication problems [4,5]. An extensive theoretical analysis of the gain, frequency bandwidth, and saturation output

power of double heterostructure laser amplifiers was made possible because of the inclusion of multimode rate equations [6]. More recently, an interest in high-data-rate systems and a requirement to determine the cross interference of various frequency modes in the lasers has stimulated a reconsideration of intraband relaxation processes. M. Yamada and Y. Suemetsu [7] considered these processes in a density matrix formulation of the problem of gain suppression in undoped injection lasers. A similar analysis was performed by R. Kazarinov, C. Henry, and R. Logan [8].

With the advent of techniques used to suppress regeneration, interest has also risen in the traveling wave amplifier (TWA). Luk'yanov et al. [9] obtained experimental results on a TWA by orienting a stripe homojunction laser at an angle to the cleaved end faces of the crystal. An analysis was made of the amplifier as a function of the pumping rate and input signal. Small signal gains exceeding 10^3 were reported. Otsuka [10] proposed and theoretically investigated laser-amplifier-based integrated optical circuits by means of simplified TWA rate equations without intraband processes included.

In this report the theory of Icsevgi and Lamb [11] is applied to the semiconductor TWA; it differs from previous work by retaining the effect of the intraband relaxation on the gain. In this report, for the first time, phase has been considered in an analysis of heterojunction amplifiers. The results of this study are important to the design of amplifiers that must produce an output in which phase is fixed with respect to the input phase and few multiple-pulse effects are exhibited. These amplifiers may be useful in heterodyne or homodyne communication systems, as components of a phase locked oscillator-amplifier high power laser source, and for optical signal processing.

B. Summary of Results

The phase of the output relative to the input is strongly dependent on frequency, the intraband collision induced homogeneous broadening, and the instantaneous density of states of the semiconductor. It is indeed possible to obtain a zero phase change for the amplified signal. Small signal gains greater than 10^3 are predicted, in agreement with Ref. 9. Saturation of intensity will occur as a consequence of the model. The effect of current limiting, introduced by a resistance (occurring naturally or introduced to prevent diode burnout) in series with the junction, is demonstrated to reduce the gain of the amplifier. For pulsed operation, the amplifier introduces pulse compression, as expected, and also introduces a nonuniform phase variation with time. This variation may limit phase coherency of the output with respect to the input field. Multi-pulse effects will be exhibited for pulse separations shorter than several pumping times.

C. Theoretical Assumptions

Following Icsevgi and Lamb [10] a self-consistent semiclassical description of the interaction between matter and radiation field is used in which the medium is treated quantum mechanically and the radiation field is treated according to Maxwell's theory. The investigation is carried out in this manner because, in contrast to the approaches of Refs. 4, 5, 6, 8 and 9, the phase can be included. Saturation occurs as a consequence of the model, and the intraband relaxation processes can be introduced in a more physical way. The starting point of the analysis is the density matrix equations, which include the phenomenological rate constants. The sources of various terms in the equations are discussed.

Self-consistency is invoked by requiring that the electric field propagating in the medium introduce a macroscopic polarization which, in turn, acts as a source term to Maxwell's equations. The following assumptions are made to simplify the problem.

1. The electromagnetic field E(z,t) is a scalar representing a uniform plane wave polarized in the x direction and propagating in the z direction. Questions concerning regeneration and modal structure, therefore, are ignored and a TWA analysis is performed.

2. Amplification in a standard double heterostructure device is considered. The medium consists of a group of two-level electron states generated by applying a bias voltage across a P-n-N junction. The conduction and valence band occupations are described by the Fermi-Dirac distribution functions. Electron transitions between two energy level distributions, rather than between two discrete levels, must be considered for interband absorption or emission of radiation at a given frequency. To further simplify the problem, the parabolic band approximation is made and it is assumed that the k-selection rule is valid. This choice will not significantly affect the spontaneous emission spectrum for energies greater than the band gap energy, which establishes the relationship between the circular frequency ω of a given transition and its corresponding wavenumber k as

$$\hbar\omega = E_g + \frac{\hbar^2 k^2}{2m_r} \tag{1}$$

where E_g is the band-gap energy, m_r is the reduced mass, and $\hbar$ is Planck's constant divided by 2π. Amplification will generally occur in a

frequency band bounded by the band-gap and the difference between quasi-Fermi levels of the conduction (F_c) and valence (F_v) bands.

$$E_g < \hbar\omega < F_c - F_v \tag{2}$$

It will be seen later, for steady state, that the gain and phase of the wave is a convolution integral of a collision line profile and a density of single particle states. For this reason the parabolic and k-selection rule assumptions are not as restrictive as it first seems since other models for the band structure, such as those postulated by Laser and Stern [11], could easily be substituted into the final results. On the other hand, the model postulated by Aleksanian, et al. [12] could not be easily used, because single particle states are not assumed for that analysis.

3. The dipole approximation holds for the interaction between the radiation field and the electronic states.
4. The two-level states are coupled only through their interaction with the common electromagnetic field E(z,t).
5. Phenomenological rate constants are included to describe the effects of pumping, spontaneous emission, and phonon-electron or electron-electron collision induced intraband decay. Interband collision-induced decay is not included, because it would make the problem only slightly more difficult and not reveal significantly more information.
6. The optical frequency ω representing a given transition is larger than the optical linewidth.

7. The rotating wave approximation applies, i.e., terms involving the creation of a photon and simultaneous creation of the upper state leading to harmonics of the optical field are ignored. Optical harmonic generation is, therefore, excluded.
8. The slowly varying wave approximation is invoked.
9. All pulses of interest are considerably longer than the intraband relaxation time.

In Section II, equations describing the phase and amplitude behavior of waves propagating in the heterojunction device are given. Numerical results are presented in Section III, and a brief summary appears in Section IV.

The appendix contains a more detailed derivation of the theory presented in the main body of the text. Note that there is a notational difference from the main text. In particular, subscripts 2 and 1 of the text are c and v in the appendix. The discussion pertaining to the calculation of a finite phase change on amplification is not included in the appendix.

II. THEORY

A. General Equations

The density matrix is introduced to represent the state of the two levels assumed for the medium. Following Icsevgi and Lamb [10], the equations of motion in component form for the density matrix are derived using Schrodinger's equations and the dipole approximation as

$$\frac{\partial \rho_2}{\partial t} = -\gamma_p(\rho_2 - \rho_{2o}) - \gamma_s \rho_2 - i\left(\frac{pE}{\hbar}\right)(\rho_{21} - \rho_{12}) \tag{3}$$

$$\frac{\partial \rho_1}{\partial t} = -\gamma_p(\rho_1 - \rho_{1o}) + \gamma_s \rho_2 + i\left(\frac{pE}{\hbar}\right)(\rho_{21} - \rho_{12}) \tag{4}$$

$$\frac{\partial \rho_{21}}{\partial t} = -(\gamma_{21} + i\omega)\rho_{21} - i\left(\frac{pE}{\hbar}\right)(\rho_2 - \rho_1) \tag{5}$$

$$\rho_{21} = \rho_{12}^{*} \tag{6}$$

where ρ_2 is the density of upper states at time t, macroscopic position z [6], and energy level or momentum k. The upper level represents a minority carrier electron in the conduction band and a corresponding hole in the valence band. The density of lower states, corresponding to an empty state in the conduction band and an electron in the valence band, is represented by ρ_1. The electromagnetic field is represented by E. The contribution to the total polarization caused by a given k state produced by the above density of states is given by the partial polarization

$$P(k,z,t) = p[\rho_{21}(k,z,t) + c.c.] \tag{7}$$

where p is the expectation value of the dipole moment.

The other terms in Eqs. (3) through (6) γ_{21}, γ_s, γ_p, ρ_{2o}, and ρ_{1o} have been introduced phenomenologically as indicated in assumption 5. The dephasing rate γ_{21} is the inverse of the dipole moment relaxation time T_2. This rate is determined by the intraband relaxation processes including polar-optical-phonon inelastic scattering, ionized impurity and heavy-hole elastic scattering, and electron-electron inelastic scattering [13]. At high doping levels and high levels of injected carriers the dominant scattering process is electron-electron. Because this process is relatively insensitive to energy level [14], the dephasing rate is assumed independent of k in this report. We note that the introduction of the intraband relaxation rate by means of Eqs. (3) through (5) is equivalent to the assumption of an exponential decay to equilibrium. In Section II.B, this assumption is modified to obtain a finite phase.

Steady-state pumping of the amplifier is accomplished by maintaining a constant bias across the semiconductor junction. Individual k state pumping is a complicated process [1] involving intraband relaxation processes, diffusion times for the carriers, and the instantaneous voltage across the junction. During amplification the population levels are reduced by stimulated emission. This causes a reduction in the instantaneous voltage across the junction. Because this voltage determines the quasi-Fermi levels, the fast intraband relaxation processes tend to restore the population to the instantaneous values determined by these Fermi levels. The intrinsic diode capaci-

tance, resistance, and carrier mobility as well as external circuit parameters determine the way in which these levels return to the equilibrium values in the absence of an electromagnetic optical pulse. The first attempts to accurately describe the electrical characteristics of the behavior of a diode have only recently been published [15,16]. A mathematical description of the processes would result in an additional set of equations to be solved simultaneously with Eqs. (3) through (6). However, because the optical pulse behavior rather than the detailed pumping behavior is of interest, a single pumping rate constant γ_p determined by the slowest process is used [17].

The pumping process discussed above restores the density of states to equilibrium values, ρ_{2o} and ρ_{1o}, determined by the Fermi levels in the absence of stimulated or spontaneous emission. These values are

$$\rho_{2o} = \frac{f_c(1 - f_v)}{\pi^2} \tag{8}$$

$$\rho_{1o} = \frac{f_v(1 - f_c)}{\pi^2} \tag{9}$$

where f_c and f_v are the Fermi distribution functions given by

$$f_c = \frac{1}{1 + \exp\left[\left(E_g + \frac{\hbar^2 k^2}{2m_c} - F_c\right)/KT\right]} \tag{10}$$

$$f_v = \frac{1}{1 + \exp\left[-\left(\frac{\hbar^2 k^2}{2m_v} + F_v\right)/KT\right]} \tag{11}$$

The quantities m_c and m_v are the electron and hole masses, respectively, F_c and F_v are the quasi-Fermi levels, K is Boltzmann's constant, and T the absolute temperature. The final constant expressed in Eqs. (3) and (4) is the spontaneous emission rate γ_s.

The electromagnetic field equation corresponding to the above set of equations determining the space-time behavior of the two-level states is

$$-\frac{\partial^2 E}{\partial z^2} + \mu_o \sigma \frac{\partial E}{\partial t} + n_o^2 c^{-2} \frac{\partial^2 E}{\partial t^2} = -\mu_o \frac{\partial^2 \sum_k P(k,z,t)}{\partial t^2} \tag{12}$$

where the conductivity σ accounts for any linear losses incurred in the absorbing medium, c is the velocity of light in vacuum, and μ_o is the magnetic permeability. Note that the total polarization P(z,t) enters Eq. (12) as the sum of partial polarizations P(k,z,t), whereas Eqs. (1) through (4) can be written in terms of the partial polarization of a single k state. The intrinsic polarization of the material resulting from the background crystal matrix is included in the index of refraction n_o.

Simplification of Eqs. (3) through (6) and (12) results from assumptions 6 through 8 in Section I and the use of retarded time. Assumption 8 means that the electromagnetic field can be written in terms of a slowly varying amplitude $\mathscr{E}$ and phase ϕ as

$$E(z,t) = \mathscr{E}(z,t) \cos[\nu t - \eta z + \phi(z,t)] \tag{13}$$

while the corresponding partial polarization may be written in terms of in-phase and out-of-phase components C and S, respectively, as

$$P(k,z,t) = C(k,z,t)\cos(\nu t - \eta z + \phi) + S(k,z,t)\sin(\nu t - \eta z + \phi) \quad (14)$$

where higher harmonics of the field are neglected. The circular frequency ν* has a nominal value close to the center of the bandwidth of the input pulse, whereas η is the wavenumber given by

$$\eta = \frac{n_o \nu}{c} \quad (15)$$

Finally, by using retarded time τ, z', and assumption 9, a coupled set of simultaneous equations can be written for the electromagnetic field amplitude $\mathscr{E}$ and phase ϕ as well as for the upper and lower level density of states ρ_1 and ρ_2.

$$\frac{\partial \mathscr{E}}{\partial z} = -L\mathscr{E} + 2g_n \mathscr{E} \int k^2(\rho_2 - \rho_1)\, \mathscr{L}(\omega)\, dk \quad (16)$$

$$\mathscr{E}\frac{\partial \phi}{\partial z} = \frac{g_n}{\gamma_{21}} \mathscr{E} \int k^2(\omega - \nu)(\rho_2 - \rho_1)\, \mathscr{L}(\omega)\, dk \quad (17)$$

$$\frac{\partial \rho_2}{\partial \tau} = -\gamma_p(\rho_2 - \rho_{2o}) - \gamma_s \rho_2 + \frac{\mathscr{E} S}{2\hbar} \quad (18)$$

$$\frac{\partial \rho_1}{\partial \tau} = -\gamma_p(\rho_1 - \rho_{1o}) + \gamma_s \rho_2 - \frac{\mathscr{E} S}{2\hbar} \quad (19)$$

*The inclusion of 2π in ν is from Ref. 10.

$$S = -\frac{p^2(\rho_2 - \rho_1)\mathcal{E}\mathcal{L}(\omega)}{\hbar\gamma_{21}} \tag{20}$$

$$\mathcal{L}(\omega) = \frac{\gamma_{21}^2}{\gamma_{21}^2 + (\omega - \nu)^2} \tag{21}$$

$$g_n = \frac{p^2}{2\hbar n_o^2 \varepsilon \gamma_{21}} \tag{22}$$

$$L = \frac{1}{2}\frac{\sigma}{n_o \varepsilon_o c} \tag{23}$$

where ε is the permitivity of free space and $\partial\phi/\partial t$ has been neglected compared to $\omega - \nu$. Note that approximation 9 means that the polarization is "locked" to the field. As soon as the pulse has passed a given location, the polarization at that location also drops to zero and the remaining inversion will not add energy into the tail of the pulse. This means that phenomena such as pulse ringing, as discussed by Icsevgi and Lamb [10] and Allen and Eberly [18], are excluded. Specialization to steady-state and pulsed regimes is considered next.

B. Steady State

Steady-state operation of the amplifier implies setting all time derivatives in Eqs. (16) through (23) equal to zero. This set of equations then reduces to

$$\frac{\partial I(z')}{\partial z} = -2L\ I(z') + 2g_n I(z') \int dk\ k^2\ \mathcal{L}(\omega)\ N(k,z') \tag{24}$$

$$\frac{\partial \phi(z')}{\partial z} = \frac{g_n}{\gamma_{21}} \int dk\ k^2(\omega - \nu)\ \mathcal{L}(\omega)\ N(k,z') \tag{25}$$

where the dimensionless intensity I(z') has been introduced and is defined here as

$$I = \frac{p^2 |\mathcal{E}|^2}{\hbar^2 \gamma_{21} (\gamma_s + \gamma_p)} \tag{26}$$

The population difference $N(k,z') = \rho_2 - \rho_1$ is given by

$$N(k,z') = \frac{[(\gamma_p - \gamma_s)/(\gamma_p + \gamma_s)]\, \rho_{2o} - \rho_{1o}}{1 + \mathcal{L}(\omega) I} \tag{27}$$

Note that saturation effects are given implicitly because N, appearing in the effective gain in Eq. (24), has the intensity as an inverse factor. Other steady-state theories include the effect of saturation; however, this effect was previously introduced phenomenologically and did not exhibit an integral dependence on momentum, which occurs here as a result of presence of the intraband relaxation processes. The equation for phase for the heterojunction amplifier [Eq. (25)] is original in this report.

The phase of the electromagnetic field is an expression of the real part of the index of refraction and as such is known to be finite. On the other hand, the phase as expressed by Eq. (25) is unbounded with the use of the parabolic approximation and an infinite upper limit on k. Although most authors, in discussing the dispersion relations for solids, give an integral expression for the real part of the index of refraction, they do not evaluate it [14-21], but use experimentally determined values instead. We evaluate the integral appearing in Eq. (25) to determine the phase both by multiplying the

Lorentzian profile [Eq. (21)] by a Gaussian profile to cut off the quadratically decaying tails of the Lorentzian and by setting an upper limit on momentum (k) integration. A previous inclusion of intraband relaxation processes in the calculation of gain [22] was based on many body theory [12] and the spectral weight function [24]. The Lorentzian spectral weight function used in Ref. 23 was derived assuming an exponential decay, which is consistent with Eqs. (3) through (5). This approximation is perfectly reasonable for a gain calculation but results in unbounded phase. Justification for the modification to the Lorentzian profile is based on the statistical theory of pressure broadening [24] and the use of a coulomb-screened potential [25] for electron-electron scattering. The use of the screened potential in the statistical theory of line broadening results in Gaussian decay in the wings of the line. The line center, however, decays slightly less rapidly than the Lorentzian, and the switch to Gaussian decay occurs between 10 and 40 line widths. The spectral line profile that was used in the calculation was then chosen as a Lorentzian multiplied by a Gaussian with a line width (at e^{-1}) of 20 γ_{21}.

Examination of Bloom and Margenau's quantum theory of spectral line broadening [26] reveals that the optical field causes transitions between "collision-smeared" states. The amount of smearing is obviously energy dependent. If there are no free electrons above a given energy level, smearing beyond that energy is not possible. The Fermi distribution for electrons in the conduction band effectively determines the maximum energy electrons that can occur and thereby determines the upper level on the k-integration. This upper limit was chosen at 9.1×10^6 cm^{-1}, which yields a value of 0.01

for the conduction-band Fermi function. It is interesting to note that this energy cutoff is consistent with the potential energy of electrons separated by a screening distance of 30 Å given for an electron density of 10^{18} [27]. This was the screening distance used in determining the Gaussian profile discussed above.

To permit numerical predictions, the dipole moment p must be determined. From Ref. 28 we can write

$$p = \left[\frac{2\pi \bar{K}\epsilon_o n_o c^3}{\omega(2m_r)^{3/2}}\right]^{1/2} \tag{28}$$

where $\bar{K}$ is an absorption parameter experimentally measured as 6000 cm^{-1} $(eV)^{-3/2}$. For values of reduced mass m_r and the transition energy given in Ref. 28 and with $n_o = 3.62$, the dipole moment p is 5.62×10^{-27} C·cm, which is equivalent to a charge separation distance of 3.5 Å.

Numerical solutions to the steady state are presented below, after the theoretical derivation for pulsed operation of the amplifier is considered.

C. Pulsed Operation

For pulses with rise times of the order of 1 psec or greater, examination of Eqs. (16) through (22) and a little algebra give a formal solution for the population difference N as

$$N(k,z',\tau) = \{N_{int} + (\gamma_p N_o - \gamma_s Q_o)\int_0^\tau d\tau' \exp[(\gamma_p + \gamma_s)\tau' + \frac{p^2 \mathscr{L}(\omega)}{\gamma_{21}^2}\int_0^{\tau'} |\mathscr{E}|^2 d\tau'']\}$$

$$\times \exp-[(\gamma_p + \gamma_s)\tau + \frac{p^2 \mathscr{L}(\omega)}{\gamma_{21}^2}\int_0^\tau |\mathscr{E}|^2 d\tau'] \tag{29}$$

Between pulses, with zero electric field, the solution for N becomes

$$N(K,z',\tau-\tau_o) = \{N_{int}(\tau_o) + \frac{(\gamma_p N_o - \gamma_s Q_o)}{\gamma_p + \gamma_s}[\exp(\gamma_p + \gamma_s)(\tau - \tau_o) - 1]\}$$

$$\times \exp -[(\gamma_p + \gamma_s)(\tau - \tau_o)] \tag{30}$$

where

$$N_o = \rho_{2o} - \rho_{1o} \tag{31}$$

$$Q_o = \rho_{2o} + \rho_{1o} \tag{32}$$

and N_{int} is the population difference at the beginning of the pulse or at time τ_o. At time zero this population difference is

$$N_{int}(k,z',0) = \left(\frac{\gamma_p - \gamma_s}{\gamma_p + \gamma_s}\right) \rho_{2o} - \rho_{1o} \tag{33}$$

If the complex field $\mathscr{E}'$ is defined as

$$\mathscr{E}' = \mathscr{E} \exp i\phi \tag{34}$$

then Eqs. (16) and (17) are written as

$$\frac{\partial \mathscr{E}'}{\partial z'} = -L\mathscr{E}' - \frac{g_n \mathscr{E}'}{\gamma_{21}} \int \frac{k^2 dk\ N(k,\tau,z')}{\gamma_{21} + i(\nu - \omega)} \tag{35}$$

III. NUMERICAL RESULTS AND DISCUSSION

A. Steady State

Table I shows the parameters used to determine the semiconductor device properties. We have also taken a typical spontaneous emission rate γ_s as 10^9 sec^{-1}, the equivalent pumping rate γ_p as 5×10^9 sec^{-1} [17], and the intraband relaxation rate γ_{21} as 10^{13} sec^{-1} [13]. Table II gives the input field frequencies, input field power (intensity), semiconductor bulk loss, and assumed device series electrical resistance for each case presented in this report. Note that in the results presented the words intensity and power are interchangeable, because the units of intensity are in watts per square micrometer and 1 μm^2 of output area is assumed. The line width (at e^{-1}) of the Gaussian profile used to cut off the Lorentzian profile tails was taken as 2×10^{14} sec^{-1} for most of the cases presented. Exceptions are noted. As a convenience, the calculated small signal gain for each case is listed in Table II.

The steady-state cases presented were calculated using a fourth-order Runge-Kutta algorithm for the differential Eqs. (24) and (25) and by using a two-point Gaussian quadrature with automatic accuracy checking to evaluate the integrals appearing in those equations. Rapid calculation was made possible by evaluating the integrals at fixed values of dimensionless intensity [Eq. (26)] and approximating the results by fourth-degree polynomial in $(1+I)^{1/2}$, including negative powers of 1/2 and 1.

Examples for steady state were chosen to demonstrate the effect of input optical field frequency, semiconductor bulk loss, the use of the Gaussian profile to cut off the Lorentzian line tails, and the effect of inserting an electrical resistance in series with the semiconductor device. Figures 1 and

Table I

ASSUMED DEVICE PARAMETERS

	P-Region	n-Region/Active	N-Region
Dimensions (active region)		0.25 μm thick, 4 μm wide, 500 μm long	
Doping level	10^{18} Ge	10^{14}	10^{18} Sn
Al concentration	45%	20%	45%
Band gap	1.985 eV	1.6734 eV	1.985 eV
m_r		0.07243 m_o (m_o electron mass)	
m_c		0.0836 m_o	
m_v		0.542 m_o	
F_c		0.1852 eV above conduction band edge	
F_v		0.0172 eV above valence band edge	
Bias	0.0193 V	1.798 V	0.0191 V

Table II

OPTICAL INPUT PARAMETERS AND CALCULATED RESULTS

	Case						
	Steady State					Pulsed	
	1	2	3	4	5	6	7
Frequency	4.046×10^{14} Hz	4.333×10^{14}	4.28×10^{14}	4.2176×10^{14}	4.197×10^{14}	4.297×10^{14}	4.297×10^{14}
Input Power	0.01 mW	0.1 mW	0.1 mW	0.1 mW	0.1 mW	0.44 mW 3×10^{10} V/m peak	0.44 mW 3×10^{10} V/m peak
Bulk loss, cm^{-1}	20	20	20	200	20	200	200
Gaussian line width, sec^{-1}	2×10^{14}	2×10^{14}	2×10^{14}	2×10^{14}	2×10^{14}	2×10^{14}	2×10^{14}
Series resistance	none	none	none	none	a) 0 b) 0.5 ohm	none	none
Small signal gain (calculated), cm^{-1}	189.8	1030.3	1014	947.7	912.22 897.9	1023	1023

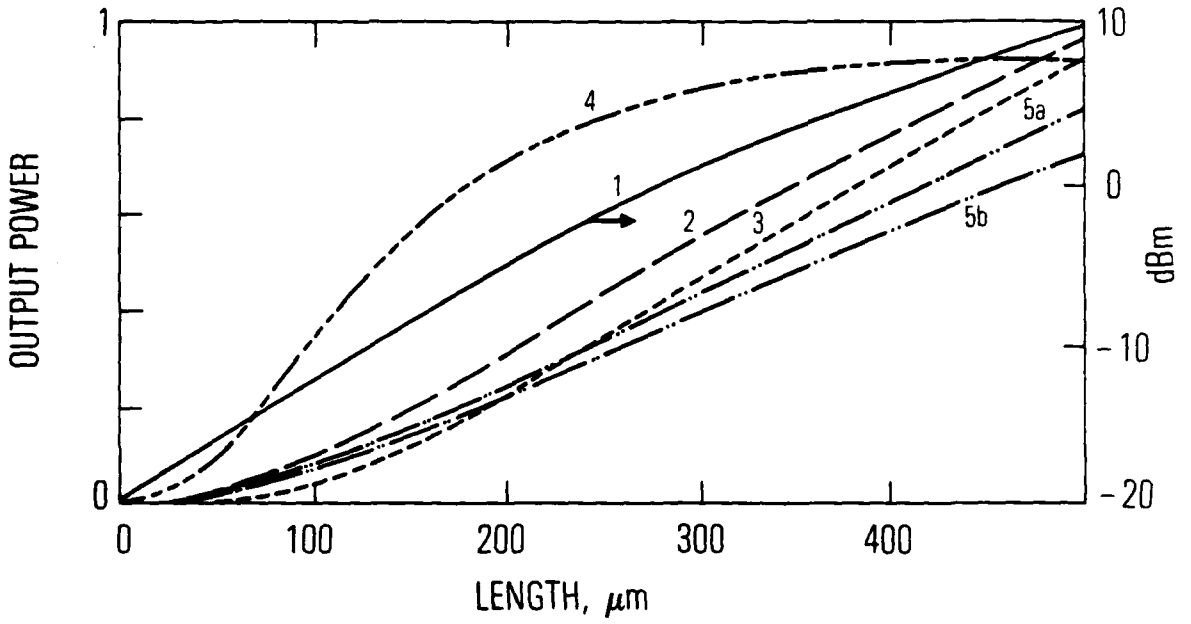

Fig. 1. Steady-state intensity response of a GaAs amplifier. Input parameters are listed in Table II. For case 1, use dBm scale on right. For cases 2, 3, 4 and 5, scale factors are 160, 160, 15, and 160 mW, respectively. Case 5b has 1/2-ohm resistance in series with junction.

2 show the intensity (power) and phase, respectively, for the five steady-state cases listed in Table II. The vertical scales have been normalized so that all five cases may be presented in the same figure. In Fig. 1, a decibel scale is used for case 1, whereas for the other cases a linear scale is used. Case 1 is an example of the small signal regime. The frequency chosen corresponds exactly to the band gap energy and is at the lower end of the frequency range for amplification expressed by Eq. (2). Without intraband relaxation processes, the gain at this frequency would be zero; however, collisions permit contributions to the gain at k equal to zero from transitions at higher k states. As seen from Fig. 1, the intensity is linear with device length, as expected for a decibel scale, until the intensity reaches the 2 to 3 $mW/\mu m^2$ range, at which point saturation effects occur. Saturation effects are also apparent for the phase shown in Fig. 2. Here the phase first increases linearly, then the slope decreases as saturation occurs.

We also considered the other end of the so-called allowed frequency range for amplification, at the frequency corresponding to the difference of quasi-Fermi levels. Although it is not shown as a case, the gain was calculated to be negative. If Eq. (2) were strictly valid, this gain would be zero; however, because of a finite pumping rate and intraband relaxation, a fairly large absorption results. Case 2 is calculated at a transition frequency giving the largest small signal gain. For this case, Fig. 1 shows a rapid transition from the small signal regime to a linear gain region. The phase, shown in Fig. 2, is negative for this case, which is not surprising because we have convolved the population difference with the standard expression for the real part of the susceptibility (Ref. 28, p. 154) of a single state. This

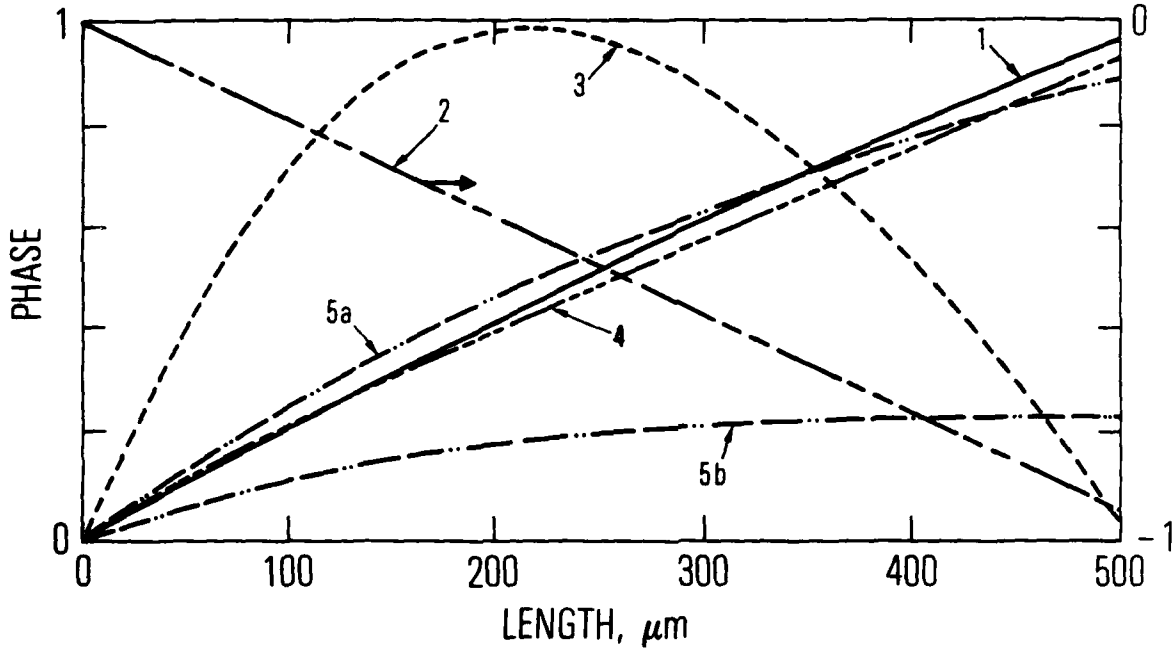

Fig. 2. Steady-state phase response of a GaAs amplifier. Scale factors for cases 1, 3, 4, and 5 are 14, 0.17, 5, and 5 rad, respectively; for case 2, scale factor on the right is 4 rad.

susceptibility is known to be antisymmetric about the resonance. If there were no upper limit on the k integration, or if the Gaussian cutoff were not used, this phase would approach negative infinity. A switch in sign for the phase between cases 1 and 2 indicates that there is a frequency that yields a zero phase change for the amplifier. That this is true is shown for case 3, with an input frequency of 4.28×10^{14} Hz. The intensity for case 3 shown in Fig. 1 is similar to that for case 2 but with a slightly smaller gain. The phase is very interesting in that there is a sign change with device length. As the intensity of the optical field grows in the amplifier, the effective homogeneous line width also increases. This permits contributions of higher k states resulting in a net decrease in the phase rather than an increase as in the small signal regime. Note that the frequencies for maximum gain and zero phase change are not the same.

Case 4 demonstrates strong saturation effects. The frequency is close but not exactly equal to that used for the examples for the pulsed operation of the amplifier. This frequency was chosen to be slightly different than for the zero phase case, because zero phase requires longer computation times. The bulk loss was increased to show saturation. The intensity shown in Fig. 1 saturates rapidly to a value of 14 $mW/\mu m^2$. The phase for this case exhibits two linear regimes; the first is for the small gain regime where the intensity is close to zero, and the second is in the region where the intensity has saturated to its final value.

For case 5, we considered the effect of placing an electrical resistance in series with the semiconductor device to limit the current drawn by the

semiconductor during amplification. This resistance may either be intrinsic to the device or included in the associated external circuit. The bias voltage across the junction drops during amplification because of this series resistance, permitting a decrease in the quasi-Fermi levels, which implies that the device will exhibit less gain than for the unrestricted or no resistance case. The effect of placing a 1/2-ohm resistance in series with the amplifier is shown as case 5b in Figs. 1 and 2. The corresponding no resistance case is 5a. As expected, the small signal gain decreases, but only slightly. On the other hand, the phase decreases by a factor of 2, and it appears that the phase saturates, whereas for the noncurrent-limited case phase continues to increase with the length of the amplifier.

To test the model dependence on the various parameters we have used, several cases were run with parameters different from those given above. These cases are shown in Figs. 3 and 4 and the parameters used are indicated in Table III. Cases presented are labeled 1, 2a, 2b, and 2c. Cases 1 and 2a are to be compared with cases 1 and 2 above, respectively, whereas cases 2b and 2c are to be compared with each other, case 2a, and case 2 above. Note that cases 2a, b, and c are for the same frequency. Cases 1 and 2a were calculated with a collisional relaxation rate 2.5 times higher than used previously. Corresponding to this relaxation rate, the Gaussian linewidth was taken as $20\ \gamma_{21}$ or 5×10^{14} Hz. The increase in linewidth for both the Lorentzian and Gaussian profiles permits a larger range of k-states to contribute to the gain and phase integrals [Eqs. (24) and (25)]. This means that the small signal gain will increase for case 1 and decrease for case 2a compared to that seen for cases 1 and 2 above, respectively. This is verified

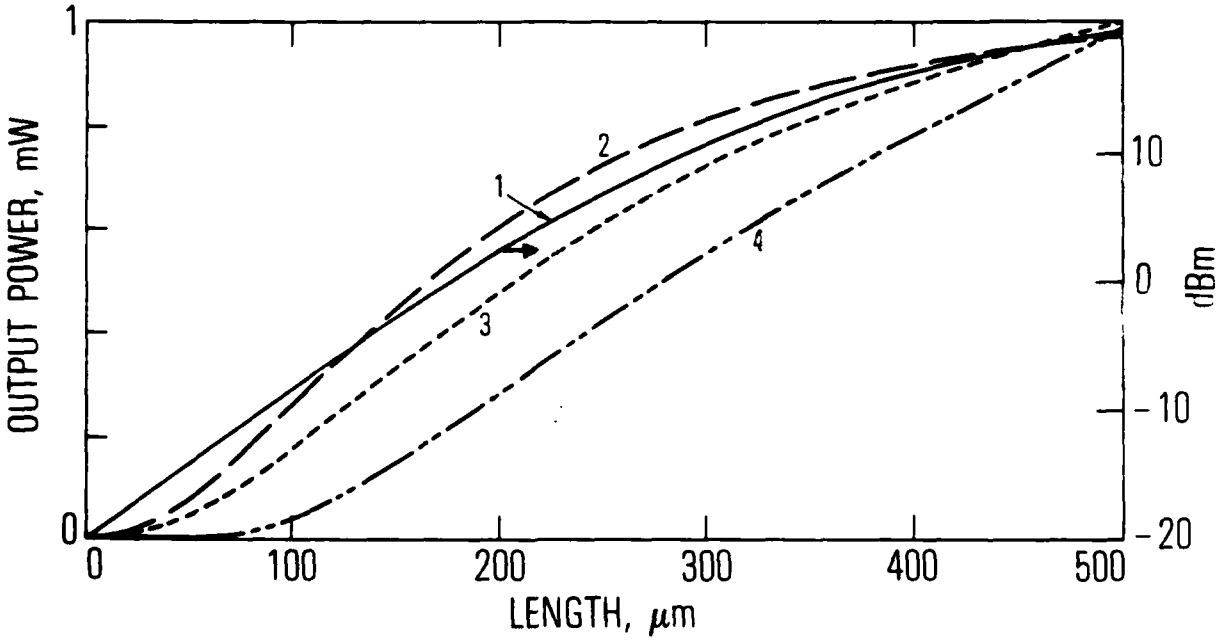

Fig. 3. Steady-state intensity response of a GaAs amplifier. For case 1, use dBm scale on right. For cases 2, 3, and 4, scale factors are 70, 70, and 240 mW, respectively. Table III shows input values.

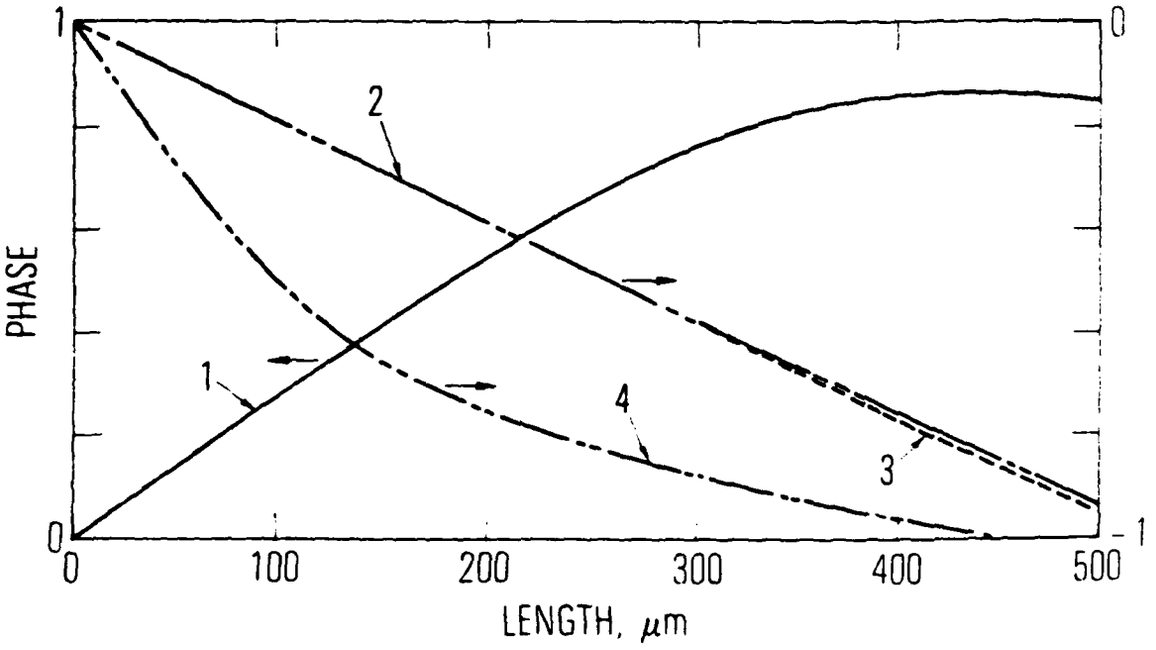

Fig. 4. Steady-state phase response of a GaAs amplifier. Alternative data set (Table III). For case 1, use scale on left; scale factor = 4 rad. For cases 2, 3, and 4, use scale on right; scale factors = -50, -30, -0.3 rad, respectively.

Table III

ALTERNATE OPTICAL INPUT PARAMETERS AND CALCULATED SMALL SIGNAL GAIN

	Case[a]			
	1	2a	2b	2c
Frequency	4.046×10^{14} Hz	4.333×10^{14} Hz	4.333×10^{14} Hz	4.333×10^{14} Hz
Input power	0.01 mW	0.25 mW	0.1 mW	0.1 mW
Bulk loss	20/cm	20/cm	20/cm	20/cm
21	2.5×10^{13}/sec	2.5×10^{13}/sec	10^{13}/sec	10^{14}/sec
Gaussian line width	5×10^{14}/sec	5×10^{14}/sec	infinity	infinity
Upper limit momentum integration	9.1×10^{6}/cm	9.1×10^{6}/cm	9.1×10^{6}/cm	6.47×10^{6}/cm
Small signal gain	247.5/cm	872.3/cm	947.7/cm	651.5/cm

[a]Steady state

by calculating the small signal gains listed in Table III. The gain for case 2a decreases, because the inclusion of more k-states in the gain integral averages in states of lower gain. The inclusion of lower gain k-states increases with intensity, resulting in intensity saturation at a value of 70 $mW/\mu m^2$, as can be seen from Fig. 3. Phase is also affected by the inclusion of added k-states. The phase for case 1 reaches a maximum and decreases, which is similar to the phase behavior for case 3, although the peak phase is considerably larger (3.5 rather than 0.17 radians). The phase for case 2a decreases much more rapidly than for case 2, reaching a value of nearly -30 radians as compared to -4 radians (Fig. 4).

To verify a prediction of very large phase in the absence of the Gaussian cutoff, we recalculated case 2 (case 2b) above for a relaxation rate of 10^{13} Hz but eliminated the Gaussian cutoff. As expected the phase decreases rapidly--12 times faster than previously. The intensity also shows saturation effects caused by the removal of this cutoff. The last case shown, 2c, was a modification of 2b. The relaxation rate was increased by a factor of 10 to 10^{14} Hz but the range of k-states permitted to contribute to the gain and phase was restricted by lowering the upper limit on the k integration by 30% to 6.47×10^6 cm^{-1}. This k cutoff corresponds to that value of k for which the direct (Γ) and indirect (χ) band energies are the same. The small signal gain for 2c decreases with respect to 2b by about 30%. Note that the scale factor for phase in Fig. 4 is only 0.3 for case 2c, indicating a very small phase variation for this case because of the nearly symmetric inclusion or k-states with positive and negative contributions to the phase integral (Eq. 25). Case 5 (not shown) with and without a series resistance was

recalculated for $\gamma_{21} = 10^{14}$/sec, no Gaussian tail cutoff, and the k upper limit of case 4. The significant behavior difference was a decreased small signal gain and a phase change from positive to negative without and with the series resistance, respectively. A shift in population level with bias voltage explains the variation.

The model dependence on the chosen parameters indicates that experiments should be made to verify results presented here.

B. Pulsed Operation

Examples presented here demonstrate the effect of the amplifier on a pulse or a series of pulses. Pulse compression, phase nonuniformity with respect to time for the output, and multi-pulse effects are of interest. The assumed pulse shape is shown as an insert in Fig. 5. The input pulses were chosen to be 54 psec long. A sinusoid electric field with a 3×10^{10} v/m peak (peak intensity 0.44 mW/μm^2) at 29 psec and a half cycle length of 50 psec were used as the basic input. The basic shape was modified by providing a linear ramp from zero time such that this ramp was tangent to the sine at approximately 17 psec. The Gaussian shape is not causal and was not considered. Note that the exact pulse shape is not important for determining qualitative features of the model. Optical input parameters used for the calculation are shown in Table II as cases 6 and 7.

The numerical procedures used to solve Eq. (35) differ considerably from the techniques used for the steady-state case. A high-order Runge-Kutta algorithm was used to perform the z integration, whereas the trapezoidal rule was used to perform the time and momentum integration. The steps in the calculation follow. At each z step the electromagnetic field as a function of

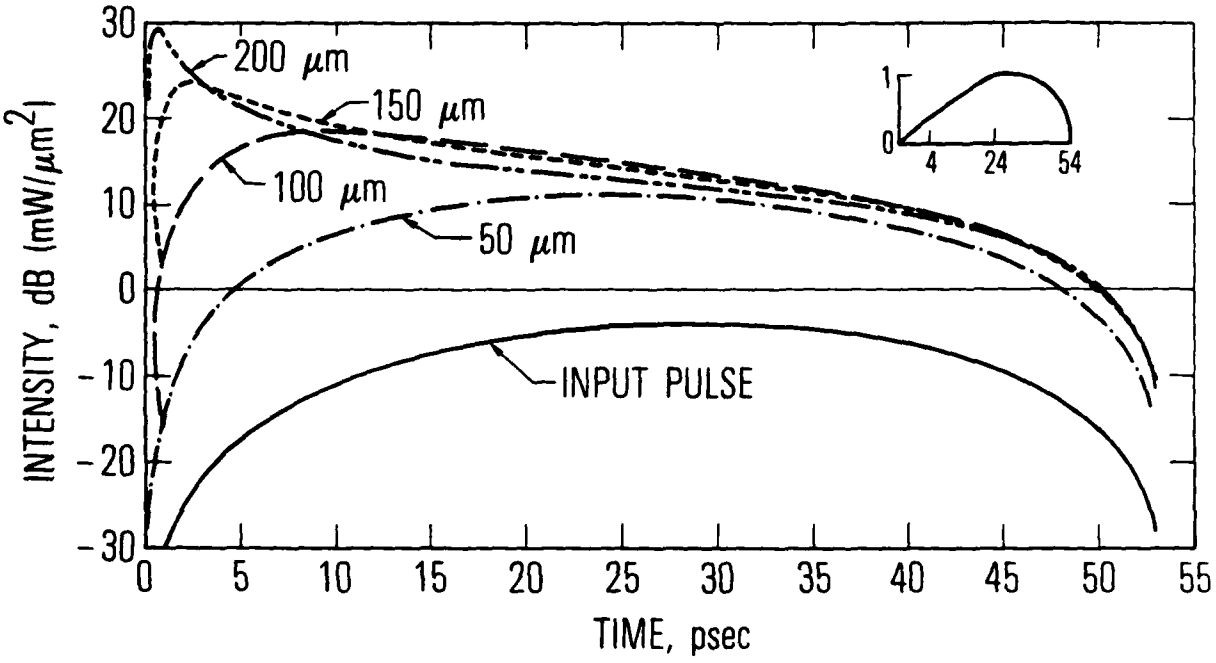

Fig. 5. GaAs amplifier intensity response to a single input modified sinusoidal pulse for various device lengths. The insert shows the input pulse amplitude shape.

time is given by the results at the previous value of z. From these values, the population inversion as a function of time and k is determined from Eqs. (29) and (30). The required input to the Runge-Kutta algorithm is completed by performing the momentum integration in Eq. (35).

Pulse compression and output phase variations with time are shown in Figs. 5 and 6. The frequency was chosen to obtain a high gain but a relatively small phase change during amplification. In these figures the curves presented are intensity or phase versus time for various values of device length as a parameter. The pulse compression shown in Fig. 5 is extreme because of the high small signal gain. The leading edge of the pulse experiences a gain of a factor of 55 for each 50-μm length, which results in a pulse compression to 2 psec in an amplifier length of 200 μm. Compression occurs because the population density is a function of the integrated intensity [Eq. (29)], so that a high intensity results in reduced gain or net absorption for the remaining pulse. Compressions shown that are less than 2 psec are probably not valid because approximation 9 no longer holds and the complete set of Eqs. (3) through (6) and (12) must be solved [10]. Note that we have attempted to limit the phase variation with time by a choice of frequency. Relative success can be seen in Fig. 6, which exhibits a phase change of approximately 0.13 radian for the 200-μm amplifier, which still amounts to a change of 30%. Other choices for frequency yield a phase change of several radians.

In Section III-A we considered the effect of a resistance in series with the heterostructure junction for a steady-state case. The effect of a series resistance on pulsed outputs is difficult to assess quantitatively with the

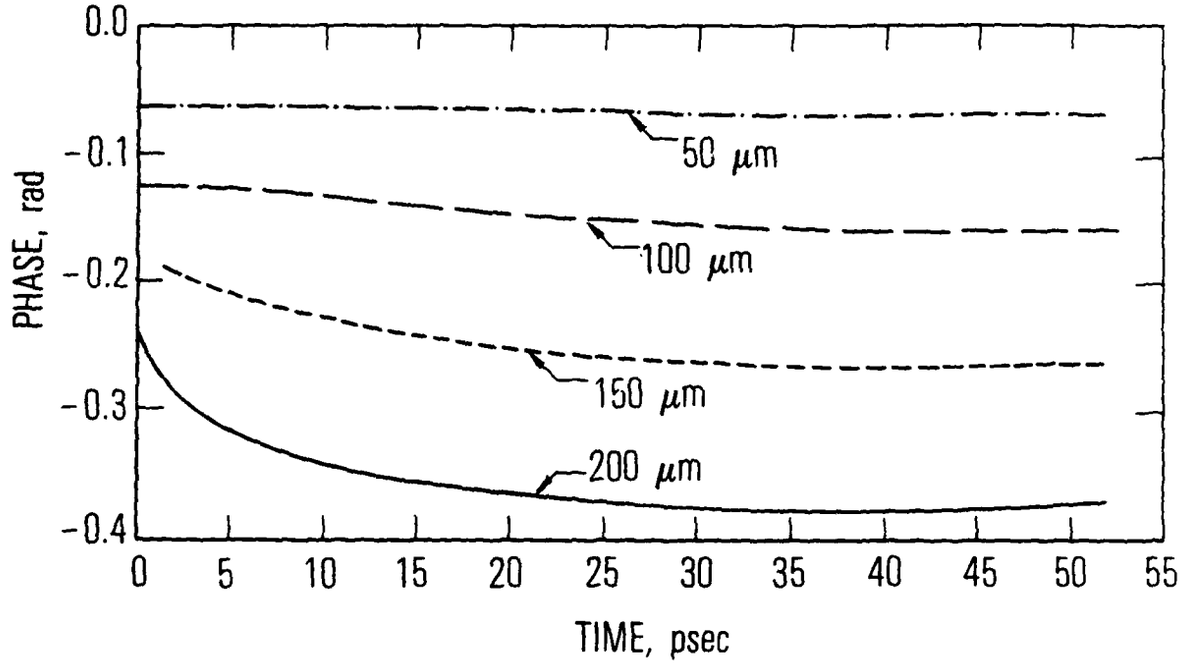

Fig. 6. GaAs amplifier phase response to a single input modified sinusoidal pulse for various device lengths.

model provided here. Qualitatively, amplification results in lowering the bias across the junction. Gain is decreased while the pulse travels through the amplifier resulting in less pulse compression and a more uniform phase than shown for Figs. 5 through 8. It would be interesting to model and calculate the effect of such a resistance as well as to perform experiments verifying such predictions.

C. Multi-Pulse Effects

For applications that require amplification of a sequence of pulses such as occur in an optical communication system, knowledge of multiple-pulse effects is of primary interest. For this study, six identical pulses were amplified in sequence by a 200-μm long device; the resulting multipulse effects are exhibited in Figs. 7 and 8. A precursor steady-state intensity of 0.01 $mW/\mu m^2$ was input to reduce the population inversion before pulse arrival. This precursor was turned off 50 psec before the first pulse arrived. The pulse sequence is illustrated in Fig. 7. The differences in output for the various pulses in the sequence are caused by the slow pumping time in relation to the pulse length and interpulse spacing. Note that there is significant inversion recovery between the third and fourth pulses. Considerable pulse-to-pulse variation occurs in phase as well as in intensity. For signal processing applications, this phase variation must be minimized by frequency choice.

From assumption 9, pulse-to-pulse interference, per se, is not possible when the pulses do not overlap. Therefore, after a pulse has passed through the amplifier, there is no residual polarization that can generate an optical field (ringing or photon echoes) as is possible when the full set of equations

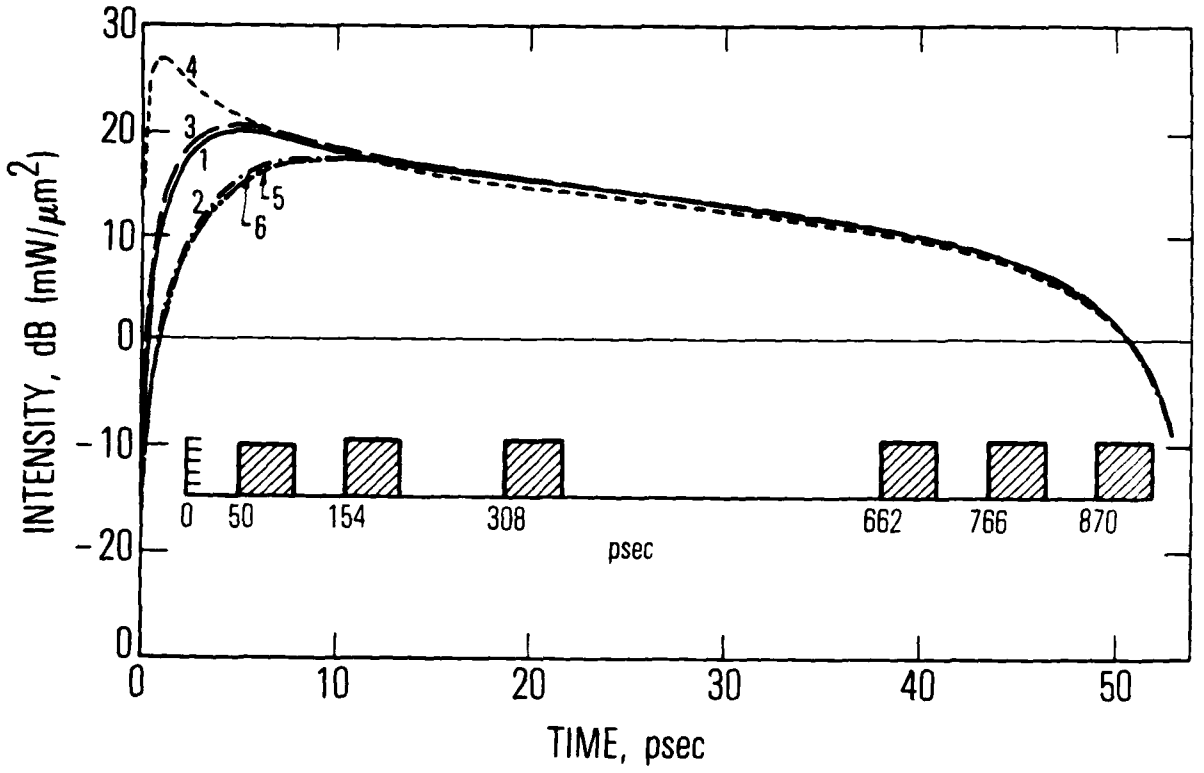

Fig. 7. GaAs amplifier intensity response to a set of six input pulses. The pulse sequence is shown in the insert. The shape of each pulse is shown in Fig. 5.

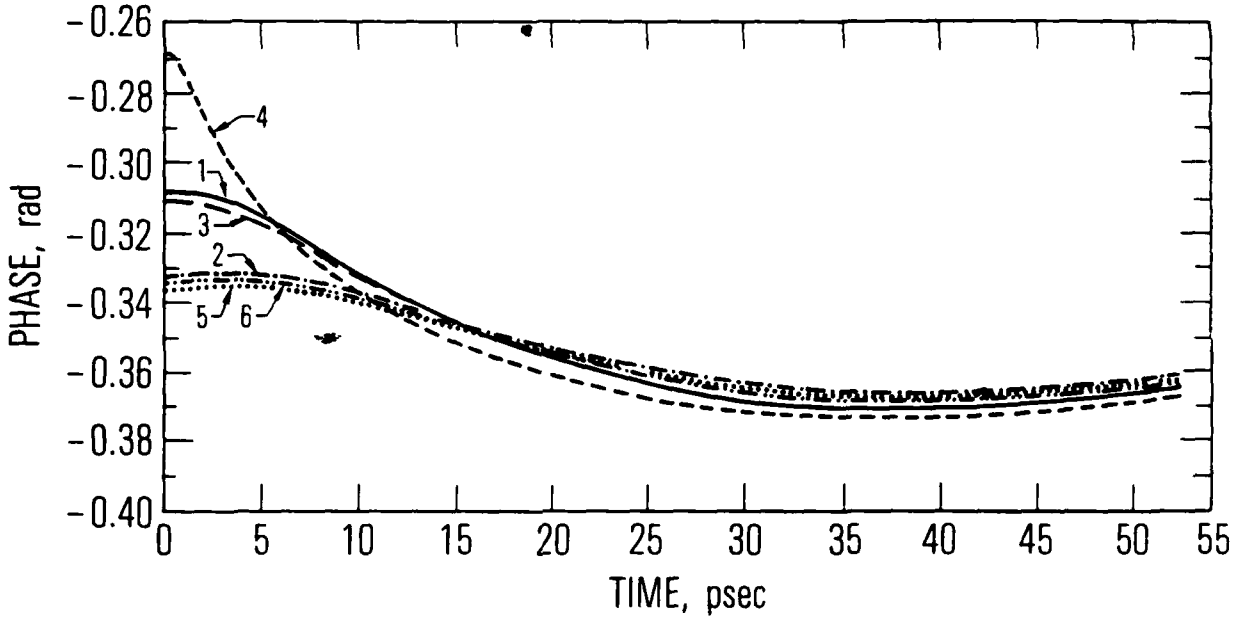

Fig. 8. GaAs amplifier phase response to a set of six input pulses.

is considered. Therefore each input pulse generates an individual output pulse based entirely on the inverted population levels at the beginning of the pulse and the input pulse shape. However, because the pumping processes generating the inverted population levels are much slower than the collisional processes, the GaAs amplifier exhibits apparent interpulse interference for repetition rates approaching 10 GHz, as shown in the figures. This occurs because there is insufficient time between pulses to build up to the signal-free inverted population levels. These effects can be avoided by limiting saturation in the amplifier by shortening the amplifier length or decreasing the available gain.

From the analysis presented, devices similar to those modeled here would amplify, compress, and show a phase variation for every pulse at a 1 Gbit rate for 50 psec pulses. These pulses would be similar to those shown in Figs. 5 and 6. Amplification of a continuous pulse train at 10 Gbits would show results similar to those shown for cases 1, 2, 5, and 6 of Figs. 7 and 8 unless at least three pulses were skipped.

For low data rates, phenomena such as pulse compression and phase change during the pulse must be compensated in applications that require uniform intensity or phase. For high data rates, a constant bit stream will keep the inverted population at a low level and produce a uniform output. For communications applications, a constant bit stream could encompass coding schemes such as polarization modulation or pulse position modulation in which the location of a pulse is shifted in time only a short distance but never deleted. On-off coding, on the other hand, skips pulses, thereby permitting

the inverted population to grow, leading to nonuniform shapes pulse-to-pulse; therefore, we suggest the use of the former coding schemes when pulse uniformity is required.

IV. CONCLUSIONS

Amplification in monolithic GaAs by means of a self-consistent semi-classical approach has been considered. Phenomenological rate constants were included to account for spontaneous emission, pumping, and collision-induced decay. Their magnitude was based on experimental evidence concerning the homogeneous line width and electron-electron induced decay times. The pumping rate constant was chosen to provide strong evidence of saturation effects in steady state in the region of 10 mW output, which seems to be justified experimentally [30].

The results obtained must be considered qualitative and not quantitative, because experiment has provided neither definitive values for the collisional relaxation rates nor the exact shape of the collision-induced emission line profile. These parameters must be determined before an accurate calculation of gain and phase change through an amplifier can be performed. Since the results presented here are model dependent, experimental results are needed to predict the behavior of the phase and gain in amplifiers.

The qualitative information available from the analysis is extensive. For the assumed range of collisional relaxation rates (10^{13}/sec to 10^{14}/sec), the use of detailed rate equations to describe optical amplification was found to be appropriate for data rates as high as 10 GHz and input pulse widths as short as 20 psec, as long as the pulses do not compress to less than 2 psec during amplification. Along with a rate equation for intensity, we have given a new rate equation for phase, which can be used in parallel with the equation

for gain. These rate equations are valid, with the assumption that the polarization follows the electric field exactly.

REFERENCES

[1] H. Haug, "Quantum Mechanical Theory of Fluctuations and Relaxation in Semiconductor Lasers," Zeitschrift für Physik, vol. 200, pp. 57-68, 1967.

[2] H. Haug and H. Haken, "Theory of Noise in Semiconductor Laser Emission," Zeitschrift für Physik, vol. 204, pp. 262-275, 1967.

[3] A. C. Scott, "Nonlinear Theory for Laser Diodes," IEEE Trans. Electron. Devices, vol. ED-11, pp. 41-46, Feb. 1964.

[4] G. Zeidler and D. Schicketanz, "Use of Laser Amplifier in Optical Glass-Fiber-Communication Systems," Siemens Forsh. Entwicklungsber, vol. 2 pp. 227-234, 1973.

[5] D. Schicketanz and G. Zeidler, "GaAs-Heterostructure Lasers as Optical Amplifiers," IEEE J. Quantum Electron., vol. QE-11, pp. 65-69, Feb. 1975.

[6] T. Mukai and Y. Yamamoto, "Gain, Frequency Bandwidth, and Saturation Output Power of AlGaAs DH Laser Amplifiers," IEEE J. Quantum Electron., vol. QE-17, pp. 1028-1034, June 81.

[7] M. Yamada and Y. Suematsu, "Analysis of Gain Suppression in Undoped Injection Lasers," J. Appl. Phys., vol. 52, April 1981.

[8] V. Luk'Yanov, A. Simenov, and S. Yakubovich, "Steady State Characteristics of a GaAs Injection Quantum Amplifier Receiving a Narrow Band Input Signal," Sov. J. Quantum Electron., vol. 10, pp. 1431-1435, Nov. 1980.

[9] K. Otsuka, "Proposal and Analysis on Laser Amplifier Based Integrated Optical Circuits," IEEE J. Quantum Electron., vol. QE-17, pp. 23-28, Jan. 1981.

[10] A. Icsevgi and W. Lamb, "Propagation of Light Pulses in a Laser Amplifier," Phys. Rev., vol. 185, pp. 517-545, Sept. 1969.

[11] A. Lasher and F. Stern, "Spontaneous and Stimulated Recombination Radiation in Semiconductors," Phys. Rev., vol. 133, pp. A553-A563, Jan. 1964.

[12] A. Aleksanian, I. Poluektov, and Y. Popov, "Theory of Optical Gain and Threshold Properties of Semiconductor Lasers," IEEE J. Quantum Electron., vol. QE-10, pp. 297-305, March 1974.

[13] M. Fleming, "Spectral Characteristics of External-Cavity-Controlled Semiconductor Lasers," Thesis, M.I.T., June 1980.

[14] C. Hearn, "Inter-Carrier Energy Exchange and the Critical Concentration of Hot Carriers in a Semiconductor," Proc. Phys. Soc. London, vol. 86, p. 881, 1965.

[15] M. Marishita, T. Ohmi, and J. Nishizawa, "Impedance Characteristics of Double-Heterostructure Laser Diodes," Solid State Electron., vol. 22, pp. 951-966, 1979.

[16] J. Katz, S. Margalit, C. Harder, D. Wilt, and A. Yariv, "The Intrinsic Electrical Equivalent Circuit of a Laser Diode," IEEE J. Quantum Electron., vol. QE-17, pp. 4-7, Jan. 1981.

[17] H. Haus, Private Communication.

[18] L. Allen and J. Eberly, Optical Resonance and Two-Level Atoms, Wiley, New York, 1975.

[19] C. Kittel, Quantum Theory of Solids, Wiley, New York, 1963.

[20] W. Harrison, Solid State Theory, McGraw Hill, New York, 1970.

[21] J. Ziman, Principles of the Theory of Solids, Cambridge University Press, p. 223, 1964.

[22] B. Zee, "Broadening Mechanism in Semiconductor (GaAs) Lasers: Limitations to Single Mode Power Emission," IEEE J. Quantum Electron., vol. QE-14, pp. 727-736, 1978.

[23] L. Hedin and S. Lundquist, Solid State Physics, F. Seitze, D. Turnbull, and H. Ehrenreich, Eds. vol. 23, Academic Press, New York, pp. 28-30, 1969.

[24] H. Margenau, "Statistical Theory of Pressure Broadening," Phys. Rev., vol. 82, pp. 156-158, 1951.

[25] C. Kittel, Introduction to Solid State Physics, Wiley, New York, p. 237, 1967.

[26] S. Bloom and H. Margenau, "Quantum Theory of Spectral Line Broadening," Phys. Rev., vol. 90, pp. 791-794, 1953.

[27] H. Casey and M. Panish, Heterostructure Lasers, Academic Press, 1978.

[28] A. Yariv, Quantum Electronics, Wiley, New York, 1975.

[29] Y. Nishimura, "Electron Scattering Times in GaAs," Jpn. J. Appl. Phys., vol. 13, p. 109, 1974.

[30] E. Garmire, Private Communication.

APPENDIX

NONREGENERATIVE OPTICAL AMPLIFICATION IN MONOLITHIC GaAs

1. INTRODUCTION

In this Appendix, a theoretical investigation of nonregenerative light amplification in GaAs double heterostructure devices is presented. The analysis is carried out from first principles. Previous analyses of GaAs devices were based on simple rate equations for laser devices. These rate equations do not contain information on the phase behavior of pulses propagated through the device nor on the range of data rates for which the theory is valid.

This investigation was carried out in conjunction with an experimental program that had the objective of developing a GaAs amplifier capable of a coherent, small signal power gain of 1000 and coherent large signal behavior. Further goals were high data rate capability without pulse-to-pulse interference effects and a large frequency range for amplification. The final goal of a large frequency bandwidth is not practical for laser amplifiers because of the Fabry-Perot or distributed Bragg reflector conditions that determine the frequency of operation. For these reasons, it was decided to examine nonregenerative optical amplification in GaAs from first principles. Nonregenerative devices are fabricated to prevent optical feedback and as such do not self-oscillate. Since there are no oscillation conditions, any frequency within the spontaneous emission bandwidth of GaAs can be amplified. Furthermore, plane wave, rather than modal analysis, is used since the optical wave passes through the device only once.

In Section 2, a detailed exposition of the theory begins, after a brief introduction, with the reduction of the material characteristics to an equivalent two-level atom problem, the introduction of the density matrix formation, and a discussion of the phenomenologically introduced decay processes. A brief discussion of the homogeneous and inhomogeneous line widths is also given. In Section 3, simplifying assumptions are made, the interaction

Hamiltonian is introduced and quantized, and the equations of motion for the density material and electromagnetic field are derived. Finally, the equations are simplified and reduced to rate equations because of the large value for the collision-induced decay processes. In Sections 4 and 5, the equations are specialized to steady-state or pulsed conditions, respectively. Device parameters and an explanation of the derivation leading to the chosen device parameters are given in Section 6. The specialization to a given set of device parameters is necessary to carry out numerical results, which are included in the main body of the text.

2. THEORY

The investigation presented in this appendix is based on a self-consistent, semiclassical approach. The electromagnetic field is treated classically, while the medium is quantized. Self-consistency is invoked by requiring that the electric field introduce a polarization in the medium which, in turn, acts as a source term to Maxwell's equation (Fig. A-1). The electromagnetic field is assumed to be a linearly polarized plane wave. The medium consists of a group of two-level electron states generated by applying a bias voltage across a monolithic P-n-N heterojunction GaAs device. The conduction and valence band occupations are described by Fermi-Dirac distribution functions. Electron transitions between the two energy-level distributions rather than between two discrete levels must be considered for interband absorption or emission of radiation at a given frequency. The dipole approximation is used to describe the interaction between the electric field and two level states. Phenomenological rate constants are included in the equations to describe the effect of pumping, spontaneous emission, and photon or electron-electron collision-induced decay. The effect of spontaneous emission noise is not included in the analysis although an understanding of this phenomenon is necessary for a complete solution to the problem. In order to quantify this problem somewhat, an actual device is contemplated.

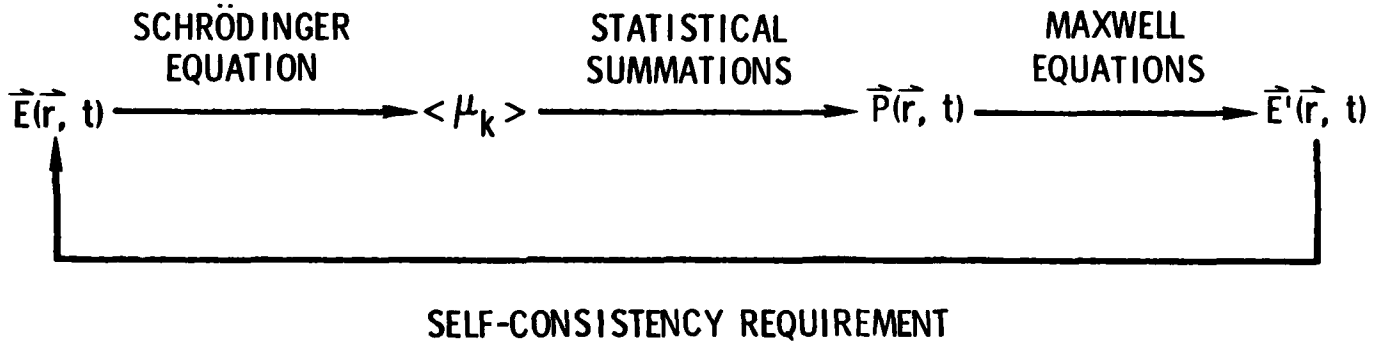

Fig. A-1. Schematic Basis for the Derivation of Equations

Let the device consist of three layers, P-n-N (shown in Fig. A-2), with doping and aluminum concentrations as indicated. The unbiased device is shown in Fig. A-2(A), and the biased device is shown in Fig. A-2(B). These figures are not drawn to scale. The details leading to these parameters are shown in Section 6 and are taken from information obtained in Ref. A-1. For simplicity it is assumed that there are no "band tails" and that the k-selection rules hold. This establishes the relationship between the circular frequency ω of a given transition and its corresponding wavenumber k as

$$\hbar\omega = E_g + \frac{\hbar^2 k^2}{2m_r} \tag{A-1}$$

where E_g is the band-gap energy (1.6734 eV) of intrinsic $Ga_{80}Al_{20}As$ at room temperature shown in Fig. A-2, m_r is the reduced mass ($7.2428 \times 10^{-2}\ m_o = 6.596 \times 10^{-29}$ g), and $\hbar$ is Planck's constant divided by 2π. A schematic representation of the direct bands, assuming a parabolic dependence on k, is shown in Fig. A-3. Note that this schematic does not correspond exactly to that shown in Fig. A-2, but corresponds more to the classic textbook representation of band models. The purpose of Fig. A-3 is to point out the parabolic nature of the bands and indicate the shape of the Fermi distributions.

The theoretical treatment follows that presented by A. Icsevgi and W. E. Lamb, Jr. (Ref. A-2) for a discrete atomic system. Since there are differences between problems with discrete atomic transitions and transitions between energy bands, we develop the theory from first principles.

As stated above, the medium is considered to be modeled using two energy bands (Fig. A-3) coupled by their interaction with an overall radiation field. If a population inversion between the conduction band and valence band can be established, the medium is capable of amplifying light in a frequency band determined by the band-gap and quasi-Fermi levels.

$$E_g < \hbar\omega < E_{F_c} - E_{F_v} \tag{A-2}$$

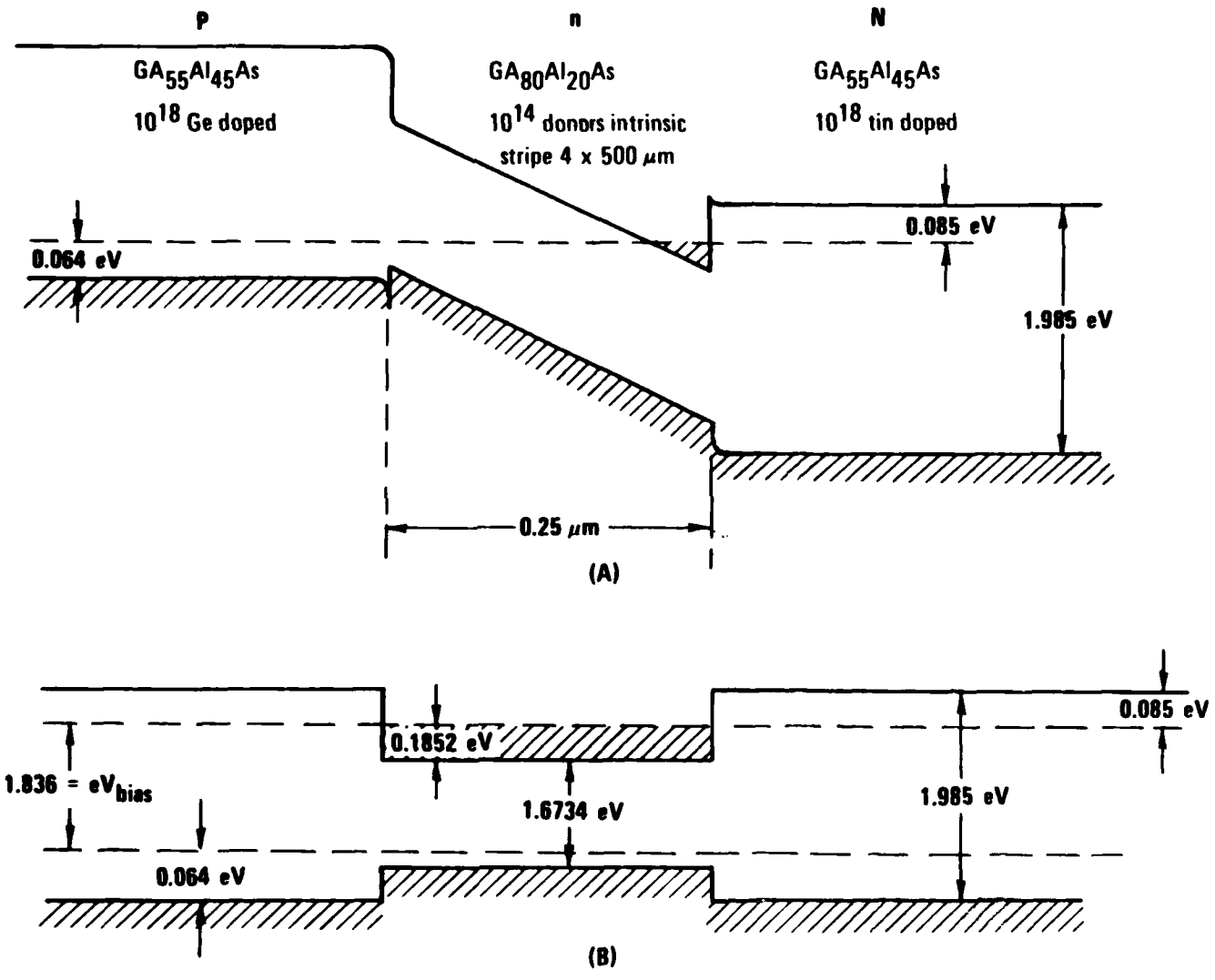

Fig. A-2. P-n-N Heterojunction Device Without and With Bias Voltage

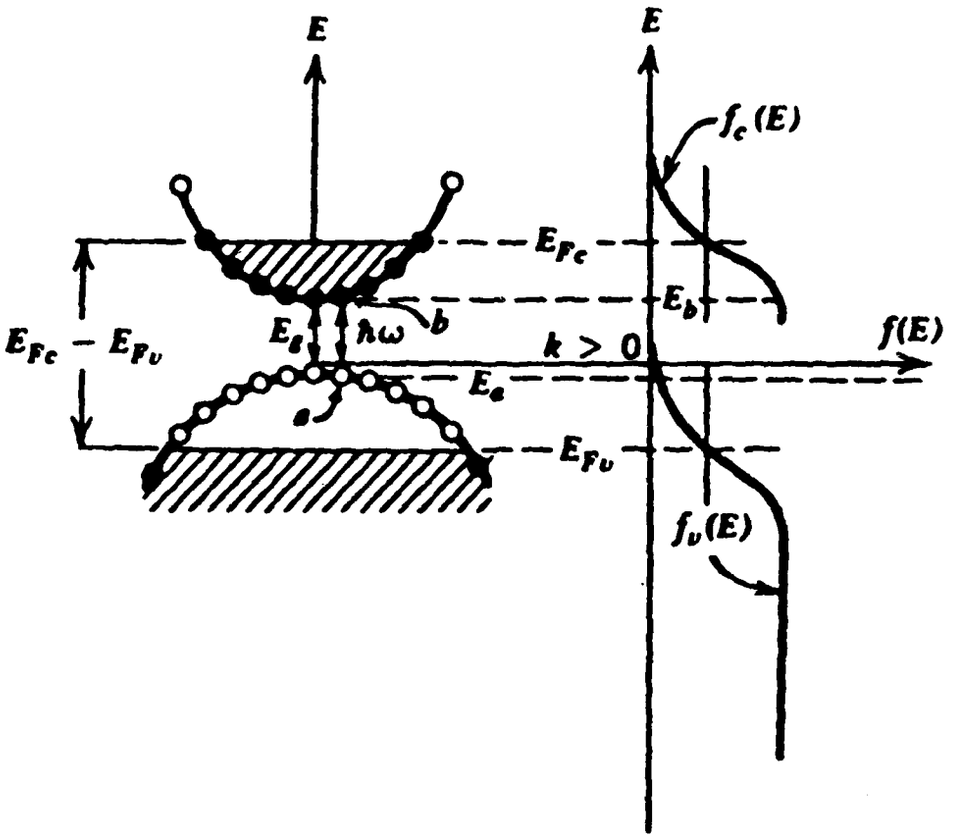

Fig. A-3. Parabolic Band Structure and Fermi Distributions

In order to carry out necessary statistical summations to eliminate unobserved variables, it is convenient to represent the conduction and valence bands as if they were levels of a two-level atom, thus obtaining equations for the density of states in either band. Following the notation for a two-level atom, it is convenient to introduce a 2 by 2 density matrix ρ. The diagonal elements will be related to the density of states in the conduction and valence bands. The upper state represents an electron in the conduction band and a corresponding hole in the valence band, whereas the lower state represents an electron in the valence band and a corresponding hole in the conduction band. The off-diagonal elements are related to the dipole moment. The density matrix is

$$\rho(t) = \begin{pmatrix} \rho_c & \rho_{cv} \\ \rho_{vc} & \rho_v \end{pmatrix} \tag{A-3}$$

The decay of levels c and v, as well as the damping of the dipole moment, must be described phenomenologically by introducing such constants as γ_s, γ_{col}, and γ_{cv}, where γ_{col} represents the decay of levels resulting from collision-induced decay, the quantity γ_s corresponds to the spontaneous emission rate, and γ_{cv} corresponds to dephasing.

Induced decay causes a population level "n" to decay as follows:

$$n(t) = n_i \exp(-\gamma_{col} t) \tag{A-4}$$

where n_i is the initial population density. At the same time, pumping will establish the population inversion. The spontaneous emission time is of the order of 10^{-9} sec, while the collision damping constant is of the order of the inverse electron-electron collision time. Since the "phase" of the dipole moment of a transition is lost when one of the upper or lower states is destroyed as a result of collision, one could say that the decay time is essentially given by γ_{col}. Associated with γ_{cv} is the (homogeneous) line width of the emission. An additional broadening exists because of the band nature of the conduction and valence bands. This establishes the inhomogeneous line

width. The entire width of the fluorescence emission is given by a convolution of the homogeneous and inhomogeneous line width. Investigations of electron-electron collision times (Ref. A-3) and the homogeneous line width (Ref. A-4), as well as private discussion,* have indicated a value of γ_{col} and therefore γ_{cv} of 10^{13} to 10^{14}. For calculations presented herein we have taken $\gamma_{col} = \gamma_{cv} = 10^{13}$. In the next section, the details of the theoretical investigation are considered. Phenomenological terms corresponding to pumping are also included there.

3. THEORETICAL DEVELOPMENT

A. ASSUMPTIONS

The calculation to be performed is summarized in Fig. A-1. The assumed electric field $\vec{E}(\vec{r},t)$ polarizes the electron in the medium. The electronic dipole moments are summed to give the macroscopic polarization $\vec{P}(\vec{r},t)$, which enters Maxwell's equation as a source term. The electric field driven by this source term must then equal the applied electric field to be self-consistent. One begins by determining the interaction Hamiltonian for the two-level states. The two-level system is quantized, and the equations of motion for the density matrix are determined. Taking into account the band nature of the amplifying medium, the expressions are summed to give the macroscopic polarization. Finally this polarization is introduced back into Maxwell's equations. In order to derive these equations, the following simplifications will be applied:

1. The two-level states are coupled only through their interaction with the common field $\vec{E}(\vec{r},t)$.

2. The radiation field is a scalar E(z,t) representing a uniform plane wave polarized in only one direction. We take this polarization direction as x with propagation in the z direction. This means the questions concerning regeneration and modal structure are completely ignored.

3. The dipole approximation holds for the interaction of the electrons with the radiation field.

*H. Haus, private communication.

4. Amplification in a double heterostructure device is being considered. The lasing region is assumed to be intrinsic GaAlAs. For this reason the parabolic band approximation is used and the only allowed transitions obey the k selection rule, i.e., transitions are between states with exactly the same momentum.

B. INTERACTION HAMILTONIAN

The classical form of the nonrelativistic Hamiltonian for a single particle of mass m and charge q moving in an electromagnetic field is given by

$$H = \frac{1}{2m} (\vec{p} - q\vec{A})^2 + q\,\phi \tag{A-5}$$

where $\vec{p}$ is the momentum conjugate to the position of the particle, $\vec{A}$ is the magnetic vector potential, and ϕ is the scalar field. The Hamiltonian is derived in the usual way (Ref. A-5), i.e., from a classical Lagrangian that includes a generalized velocity-dependent potential obtained from the Lorentz force on the particle arising from the electromagnetic field $(\vec{E},\vec{B})$. That field obeys Maxwell's equations, given here for completeness:

$$\vec{\nabla} \times \vec{E} + \frac{\partial \vec{B}}{\partial t} = 0 \tag{A-6}$$

$$\vec{\nabla} \cdot \vec{D} - \rho = 0 \tag{A-7}$$

$$\vec{\nabla} \times \vec{H} - \vec{J} - \frac{\partial \vec{D}}{\partial t} = 0 \tag{A-8}$$

$$\vec{\nabla} \cdot \vec{B} = 0 \tag{A-9}$$

Equation (A-9) implies that

$$\vec{B} = \vec{\nabla} \times \vec{A} \tag{A-10}$$

and Eq. (A-6) that

$$\vec{E} = -\vec{\nabla}\phi - \frac{\partial A}{\partial t} \tag{A-11}$$

The conversion from classical physics to quantum physics is accomplished by the replacement of the conjugate momentum $\vec{p}$ by $\hbar/i\vec{\nabla}$. For convenience $\vec{p}$ will be retained wherever possible. An additional potential energy V is added to the Hamiltonian in Eq. (A-5).

The single-particle-plus-field Hamiltonian is written in the form

$$H = H_m + H_c + H_I \tag{A-12}$$

where

$$H_m = \frac{1}{2m}\vec{p}^2 + V \tag{A-13}$$

$$H_I = \frac{q}{m}\vec{A}\cdot\vec{p} + \frac{iq\hbar}{2m}(\vec{\nabla}\cdot\vec{A}) + \frac{q^2}{2m}|\vec{A}|^2 + q\phi \tag{A-14}$$

and the final term is the energy content of the electromagnetic field

$$H_f = \frac{1}{2}\int(\vec{E}\cdot\vec{D} + \vec{H}\cdot\vec{B})d^3x \tag{A-15}$$

Since the electromagnetic strength does not vary over distances of the order of a wavelength, it is possible to sum the interaction energy over the allowed states in the conduction band with the states labeled by the momentum k

$$H_I(x) = \sum_k \{\frac{q}{m}\vec{A}(x_k)\cdot\vec{p}_k + \frac{iq\hbar}{2m}[\vec{\nabla}\cdot\vec{A}(\vec{x}_k)] + \frac{q^2}{2m}|\vec{A}(\vec{x}_k)|^2 + q\phi(\vec{x}_k)\} \tag{A-16}$$

By performing a gauge transformation, one obtains

$$\vec{A}(\vec{x}_k) \rightarrow \vec{A}(\vec{x}_k) + \vec{\nabla}_k\Lambda \tag{A-17}$$

$$\phi(\vec{x}_k) \rightarrow \phi(\vec{x}_k) - \frac{\partial \Lambda}{\partial t} \tag{A-18}$$

In order to simplify this expression, Λ is chosen such that

$$\vec{\nabla}\Lambda = -\vec{A}(\vec{x}) \tag{A-19}$$

Over dimensions of an order of a wavelength

$$\vec{A}(\vec{x}_k, t) = \vec{A}(x, t) \tag{A-20}$$

where x is the center of mass of a group of atoms with linear dimensions of the order of a wavelength. Λ is then found to be

$$\Lambda = -\vec{A}(x, t) \cdot \vec{x}_k \tag{A-21}$$

When the coulomb gauge is applied (no sources for the electromagnetic field), $\phi(\vec{x}_k)$ is set to zero; therefore

$$\vec{E} = -\frac{\partial \vec{A}}{\partial t} \tag{A-22}$$

and the interaction Hamiltonian is

$$H_I(x) = \vec{E}(z) \cdot \sum_k q\vec{x}_k \tag{A-23}$$

The quantity $q\vec{x}_k$ is recognized as the dipole moment $\vec{\mu}_k$, therefore

$$H_I = \vec{E}(z) \cdot \sum_k \vec{\mu}_k \tag{A-24}$$

C. EQUATIONS OF MOTION FOR THE DENSITY MATRIX

It is well known that the equation of motion for the density matrix for a single "pure" state labeled by k is given by (Ref. A-6)

$$i\hbar \frac{\partial \rho}{\partial t} = [H, \rho] \tag{A-25}$$

where the brackets represent the commutator and the field energy commutes with the density matrix and can be ignored in Eq. (A-25). In the representation where the electron basis functions ψ_c and ψ_v are eigenfunctions of H_m, we have

$$H_m = \hbar \begin{pmatrix} \frac{\omega}{2} & 0 \\ 0 & -\frac{\omega}{2} \end{pmatrix} \tag{A-26}$$

and

$$H_I = \hbar \begin{pmatrix} 0 & -\frac{p}{\hbar} E(t) \\ -\frac{p}{\hbar} E(t) & 0 \end{pmatrix} \tag{A-27}$$

where

$$p = (c|\mu|v) \tag{A-28}$$

is taken to be real. The diagonal matrix elements of μ vanish. In component form the equations of motion become

$$\dot{\rho}_c = -\gamma_{col}(\rho_c - \rho_{co}) - \gamma_s \rho_c - i\left(\frac{pE}{\hbar}\right)(\rho_{cv} - \rho_{vc}) \tag{A-29}$$

$$\dot{\rho}_v = -\gamma_{col}(\rho_v - \rho_{vo}) + \gamma_s \rho_c + i\left(\frac{pE}{\hbar}\right)(\rho_{cv} - \rho_{vc}) \tag{A-30}$$

$$\dot{\rho}_{cv} = -(\gamma_{cv} + i\omega)\rho_{cv} - i\left(\frac{pE}{\hbar}\right)(\rho_c - \rho_v) \tag{A-31}$$

$$\rho_{cv} = \rho_{vc}^{*} \tag{A-32}$$

where the phenomenological terms γ_s, γ_{col}, and γ_{cv} have been introduced to account for both damping and pumping. Note that pumping is established by applying a bias across the GaAs device. This bias establishes equilibrium values of the upper and lower states ρ_{co} and ρ_{vo} that would exist in the absence of spontaneous emission and an electromagnetic field. Differences from equilibrium then accomplish pumping or decay through the collision process. These equations will be modified slightly later in the report but are now sufficient to continue our discussion.

The individual electron or Bloch states may be specified by various labels, such as position z, time t, momentum k, upper or lower state (c,v), etc. Note that, since we use the envelope or slowly varying wave approximation, we may specify z and k at the same time. The dipole moment μ is given by the trace with the density, resulting in

$$\langle\mu\rangle = p[\rho_{cv}(z,t,r, \text{ etc.}) + \rho_{vc}] \tag{A-33}$$

On the other hand, Eqs. (A-29)-(A-31) depend only on z, t, and k, and the macroscopic polarization of the medium P(z,t) does not depend on k. For this reason the extra variables labeling the individual electron states are eliminated by taking the ensemble average for all states having the same t, z, and k labels, and the total polarization P(z,t) is then the sum over partial polarizations.

$$P(z,t) = \int dk P(k,z,t) = \int dk p[\rho_{cv}(k,z,t) + cc] \tag{A-34}$$

Equation (A-29) is rewritten with specific labels as

$$\partial\rho_c(k,z,t) = -\gamma_{col}[\rho_c(k,z,t) - \rho_{co}] - \gamma_s\rho_c(k,z,t)$$

$$- i\frac{p_k}{\hbar}E(z,t)(\rho_{cv} - \rho_{vc}) \tag{A-35}$$

while Eqs. (A-30) and (A-31) are written for completeness as

$$\partial\rho_v(k,z,t) = -\gamma_{col}(\rho_v - \rho_{vo}) + \gamma_s\rho_c + i\left(\frac{pE}{\hbar}\right)(\rho_{cv} - \rho_{vc}) \qquad \text{(A-36)}$$

$$\partial\rho_{cv}(k,z,t) = -(\gamma_{cv} + i\omega)\rho_{cv} - i\left(\frac{p}{\hbar}\right)E(z,t)(\rho_c - \rho_v) \qquad \text{(A-37)}$$

where ∂ represents $\partial/\partial t$.

These equations can be written in terms of the partial polarization $P(k,z,t)$ in a straightforward manner (Ref. A-2):

$$[(\partial + \gamma_{cv})^2 + \omega^2]P(k,z,t) = -2\omega\left(\frac{p_k^2}{2\hbar}\right)E(z,t)(\rho_c - \rho_v) \qquad \text{(A-38)}$$

$$(\partial + \gamma_{col} + \gamma_s)\rho_c = \gamma_{col}\rho_{co} + \hbar\omega^{-1}\,E(\partial + \gamma_{cv})P \qquad \text{(A-39)}$$

$$(\partial + \gamma_{col})\rho_v = \gamma_{col}\rho_{vo} + \gamma_s\rho_c - \hbar\omega^{-1}\,E(\partial + \gamma_{cv})P \qquad \text{(A-40)}$$

The corresponding electromagnetic equation follows immediately from Maxwell's equations, giving

$$-\frac{\partial^2 E}{\partial z^2} + \mu_o\frac{\sigma\partial E}{\partial t} + n_o^2c^{-2}\frac{\partial^2 E}{\partial t^2} = -\frac{\mu_o\partial^2 P(z,t)}{\partial t^2} \qquad \text{(A-41)}$$

where the conductivity σ accounts for any linear losses incurred in the absorbing medium, c is the velocity of light in vacuum, and μ_o is the magnetic permeability. Note that the total polarization enters Eq. (A-41), while the partial polarizations enter Eqs. (A-38)-(A-40). The intrinsic polarization of the material resulting from the background crystal matrix is included as a factor n_o, the index of refraction.

D. SIMPLIFICATION OF THE BASIC EQUATIONS

We now make two additional assumptions and remind the reader of a third already discussed.

1. The optical frequency ω is larger than the optical linewidth; therefore

$$\omega > \gamma_{cv} \tag{A-42}$$

2. The rotating wave approximation applies, i.e., terms involving the creating of a photon and the simultaneous creation of the upper state leading to harmonics of the optical field are ignored.

3. Recall that the slowly varying wave approximation has already been invoked in the description of the medium. For the electromagnetic wave this means we can write

$$E(z,t) = \mathcal{E}(z,t)\cos[\nu t - \eta z + \phi(z,t)] \tag{A-43}$$

The frequency circular ν will have a nominal value close to the center of the bandwidth of the input pulse. Different choices of ν lead to different phase functions $\phi(z,t)$. The wavenumber η will always be

$$\eta = \frac{n_o \nu}{c} \tag{A-44}$$

The amplitude and ϕ phase will vary slowly in an optical cycle and wavelength, i.e.,

$$\frac{\partial \mathcal{E}}{\partial t} \ll \nu, \quad \frac{\partial \mathcal{E}}{\partial z} \ll \eta \tag{A-45}$$

$$\frac{\partial \phi}{\partial t} \ll \nu\phi, \quad \frac{\partial \phi}{\partial z} \ll \eta\phi \tag{A-46}$$

If the field is written as in Eq. (A-43), the partial polarization may be written in terms of in-phase and out-of-phase components C and S, respectively, as

$$P(k,z,t) = C(k,z,t)\cos(\nu t - \eta z + \phi) + S(k,z,t)\sin(\nu t - \eta z + \phi) \tag{A-47}$$

where higher harmonics of the field are neglected. These approximations are substituted into Eqs. (A-38)-(A-41), yielding

$$\frac{\partial \mathcal{E}}{\partial z} + n_o c^{-1} \frac{\partial \mathcal{E}}{\partial t} = \frac{-\bar{k}\mathcal{E}}{n_o} - \frac{1}{2} \eta \int \frac{dk S(k,z,t)}{n_o^2 \varepsilon_o} \tag{A-48}$$

$$\left[\frac{\partial \phi}{\partial z} + c^{-1} \frac{\partial \phi}{\partial t}\right] \mathcal{E} = -\frac{1}{2} \eta \int \frac{dk C(k,z,t)}{n_o^2 \varepsilon_o} \tag{A-49}$$

$$\frac{\partial C(k,z,t)}{\partial t} = -\gamma_{cv} C(k,z,t) + \left(\omega - \nu - \frac{\partial \phi}{\partial t}\right) S(k,z,t) \tag{A-50}$$

$$\frac{\partial S(k,z,t)}{\partial t} = -\gamma_{cv} C(k,z,t) + \left(\omega - \nu - \frac{\partial \phi}{\partial t}\right) C(k,z,t) - \left(\frac{p}{\hbar}\right)^2 \mathcal{E}(\rho_c - \rho_v) \tag{A-51}$$

$$\frac{\partial \rho_c(k,z,t)}{\partial t} = -\gamma_{col}\left[\rho_c(k,z,t) - \rho_{co}(k,z,t)\right] - \gamma_s \rho_c(k,z,t) + \mathcal{E}(z,t) \frac{S(k,z,t)}{2\hbar} \tag{A-52}$$

$$\frac{\partial \rho_v(k,z,t)}{\partial t} = -\gamma_{col}\left[\rho_v(k,z,t) - \rho_{vo}(k,z,t)\right] + \gamma_s \rho_c(k,z,t) - \mathcal{E}(z,t) \frac{S(k,z,t)}{2} \tag{A-53}$$

$$\bar{k} = \frac{1}{2} \frac{\sigma}{\varepsilon_o c} \tag{A-54}$$

where ε_o is the permittivity of free space.

The equilibrium values of the density of states ρ_{co} and ρ_{vo} are determined by the quasi-Fermi levels. The Fermi levels are determined by temperature and the voltages maintained across the device. Expressions for these equilibrium densities are

$$\rho_{co} = \frac{f_c(1 - f_v)}{\pi^2} \tag{A-55}$$

$$\rho_{vo} = \frac{f_v(1 - f_c)}{\pi^2} \tag{A-56}$$

where f_c and f_v are the Fermi functions shown in Fig. A-3

$$f_c = \frac{1}{1 + \exp\left[\left(E_g + \frac{\hbar^2 k^2}{2m_c} - F_c\right)/KT\right]} \tag{A-57}$$

$$f_v = \frac{1}{1 + \exp\left[\left(\frac{\hbar^2 k^2}{2m_v} - F_v\right)/KT\right]} \tag{A-58}$$

We take the quantity KT as 1/40 eV. E_q is the band-gap energy of the intrinsic region and is 1.6734 eV, the quasi-Fermi level for the conduction band is 0.0172 eV, and the quasi-Fermi level for the valence band is 1.8536 eV. The mass of the electron state in the conduction band is $m_c = 7.61454 \times 10^{-29}$g, and the electron mass in the valence band $m_v = 4.9367 \times 10^{-28}$g. As long as the voltage and temperature are maintained, the equilibrium values for the population will remain constant. This issue will be addressed again later in the report.

At this point we introduce retarded time "τ," transforming to a set of new variables

$$\tau = t - z\frac{n_o}{c} \tag{A-59}$$

$$z = z \tag{A-60}$$

so that

$$\frac{\partial}{\partial z} + n_o c^{-1} \frac{\partial}{\partial t} = \frac{\partial}{\partial z}$$

$$\frac{\partial}{\partial t} = \frac{\partial}{\partial \tau} \tag{A-61}$$

and we have

$$\frac{\partial \mathscr{E}}{\partial z} = -\frac{\bar{k}\mathscr{E}}{n_o} - 1/2\ \eta \int \frac{S}{n_o^2 \varepsilon_o} \tag{A-62}$$

$$\mathscr{E}\left[\frac{\partial \phi}{\partial z}\right] = -1/2\ \eta \int \frac{C}{n_o^2 \varepsilon_o} \tag{A-63}$$

$$\frac{\partial S}{\partial \tau} = -\gamma_{cv} S - (\omega - \nu - \dot{\phi})C - \frac{p^2}{\hbar}\ \mathscr{E}(\rho_c - \rho_v) \tag{A-64}$$

$$\frac{\partial C}{\partial \tau} = -\gamma_{cv} C + (\omega - \nu - \dot{\phi})S \tag{A-65}$$

$$\frac{\partial \rho_c}{\partial \tau} = -\gamma_{col}(\rho_c - \rho_c) - \gamma_s \rho_c + \frac{1}{2}\ \frac{\mathscr{E}S}{\hbar} \tag{A-66}$$

$$\frac{\partial \rho_v}{\partial \tau} = -\gamma_{col}(\rho_v - \rho_{vo}) + \gamma_s \rho_c - \frac{1}{2}\ \frac{\mathscr{E}S}{\hbar} \tag{A-67}$$

Generally, Eqs. (A-62)-(A-67) would be the set of equations used for calculations. However, because of the size of γ_{cv} and γ_{col}, further modification and approximations are necessary. Since we will be interested in pulses whose widths are generally greater than 1 psec and γ_{cv} is of the order of 10^{13}, we can neglect the time derivatives of S and C in Eqs. (A-64) and (A-65). Further $\dot{\phi}$ can be dropped from these equations. This immediately implies that

$$S = -\frac{p^2 \mathcal{E}\gamma_{cv}}{\hbar[\gamma_{cv}^2 + (\omega - \nu)^2]}(\rho_c - \rho_v) \tag{A-68}$$

$$C = -\frac{p^2 \mathcal{E}(\omega - \nu)}{\hbar[\gamma_{cv}^2 + (\omega - \nu)^2]}(\rho_c - \rho_v) \tag{A-69}$$

One might assume that the time derivatives in Eqs. (A-66) and (A-67) could also be set to zero within the same approximation. This would imply that the density of states for the upper and lower states was essentially given by ρ_{co} and ρ_{vo}. However, we assumed initially that ρ_{co} and ρ_{vo} were determined by the voltage across the intrinsic region and that this voltage remains constant. In reality, as the population levels are drawn down because of stimulated emission, the voltage across the region changes, inducing a current flow in the device. The intrinsic capacitance, resistance, and mobility, as well as external circuit parameters, determine how the Fermi levels are restored to the equilibrium value of ρ_{co} and ρ_{vo}. This would entail the addition of extra equations to take these effects into account. As an approximation, we will replace all three extra equations and Eqs. (A-66) and (A-67) by simply changing γ_{col} to γ_p, where γ_p is an equivalent pumping rate to the system. We take $\gamma_p = 5 \times 10^9$/sec.* This gives the following set for equations:

$$\frac{\partial \mathcal{E}}{\partial z} = -L + \frac{\eta\mu^2 \mathcal{E}}{2 n_o^2 \varepsilon_o} \int \frac{dk\gamma_{cv}(\rho_c - \rho_v)}{[\gamma_{cv}^2 + (\omega - \nu)^2]} \tag{A-70}$$

$$\mathcal{E}\frac{\partial \phi}{\partial z} = \frac{\eta\mu^2 \mathcal{E}}{2\hbar n_o^2 \varepsilon_o} \int \frac{dk(\omega - \nu)(\rho_c - \rho_v)}{[\gamma_{cv}^2 + (\omega - \nu)^2]} \tag{A-71}$$

$$\frac{\partial \rho_c}{\partial \tau} = -\gamma_p(\rho_c - \rho_{co}) - \gamma_s \rho_c - \frac{\mu^2 \gamma_{cv} |\mathcal{E}|^2 (\rho_c - \rho_v)}{2\hbar^2[\gamma_{cv}^2 + (\omega - \nu)^2]} \tag{A-72}$$

*H. Haus, private communication.

$$\frac{\partial \rho_v}{\partial \tau} = -\gamma_p(\rho_v - \rho_{vo}) + \gamma_s \rho_c + \frac{\mu^2 \gamma_{cv} |\mathcal{E}|^2 (\rho_c - \rho_v)}{2\hbar^2[\gamma^2 + (\omega - \nu)^2]} \tag{A-73}$$

where we have replaced the symbol p by μ and assumed that this dipole moment μ is independent of momentum k. The limits of integration for Eqs. (A-70)-(A-71) and the value of μ will be discussed later. The quantity L represents the linear loss term and was represented by $\bar{k}/n_o$ earlier. Two regimes of operation--steady state and pulsed--are of interest. These two regimes will be considered in the following sections.

4. STEADY-STATE OPERATION

For steady-state operation, the time derivatives of ρ are set to zero, and the population difference $N = \rho_c - \rho_v$ is immediately given by

$$N = \frac{\frac{(\gamma_p - \gamma_s)}{\gamma_p + \gamma_s} \rho_{co} - \rho_{vo}}{1 + \frac{\mu^2 f(\omega) |\mathcal{E}|^2}{\hbar^2 \gamma_{cv}(\gamma_s + \gamma_p)}} \tag{A-74}$$

where

$$f(\omega) = \frac{\gamma_{cv}^2}{\gamma_{cv}^2 + (\omega - \nu)^2} \tag{A-75}$$

By defining a dimensionless intensity

$$I = \frac{\mu^2 |\mathcal{E}|^2}{\hbar^2 \gamma_{cv}(\gamma_s + \gamma_p)} \tag{A-76}$$

Eqs. (A-70) and (A-71) can be rewritten as

$$\frac{\partial I(z)}{\partial z} = -\underline{L}\, I(z) + g_n I(z) \int \frac{dk\ k^2 f(\omega)\left[\frac{(\gamma_p - \gamma_s)\rho_{co}}{\gamma_p + \gamma_s} - \rho_{vo}\right]}{1 + I(z) f(\omega)} \tag{A-77}$$

$$\frac{\partial\phi(z)}{\partial z} = \frac{g_n}{2\gamma_{cv}} \int \frac{dk\ k^2(\omega - \nu)f(\omega)\left[\frac{(\gamma_p - \gamma_s)\rho_{co}}{\gamma_p + \gamma_s} - \rho_{vo}\right]}{1 + I(z)f(\omega)} \tag{A-78}$$

where

$$g_n = \frac{\eta\mu^2}{\hbar n_o^2 \varepsilon \gamma_{vc}} \tag{A-79}$$

and

$$\underline{L} = 2L \tag{A-80}$$

The factor k^2 is shown explicitly in the integrals of Eqs. (A-77) and (A-78). The value of the dipole moment μ may be determined experimentally in an indirect fashion. It has been determined (Ref. A-7) that the quantity

$$\overline{K} = \frac{\omega\mu^2(2m_r^{3/2})}{2\pi\varepsilon_o n_o c^3} = 6000\ \text{cm}^{-1}(\text{eV})^{-1/2} \tag{A-81}$$

From the values of reduced mass and energy of transition (1.51 eV) used in that reference and an index of refraction of 3.62, the dipole moment is $\mu = 5.62 \times 10^{-27}$ coulomb -cm, which is equivalent to a separation distance of 3.5 Å. Finally, note that, if the limits of integration are allowed to go to infinity, then the integral in Eq. (A-78) is unbounded. An expanded discussion of this point has been included in the main body of the text.

5. PULSED OPERATION

Examination of Eqs. (A-70)-(A-73) leads one to make several modifications. For the steady state, we define the population difference

$$N(t,z,k) = \rho_c(t,z,k) - \rho_v(t,z,k) \tag{A-82}$$

and also the sum

$$O(t,z,k) = \rho_c + \rho_v \tag{A-83}$$

By adding Eqs. (A-72) and (A-73), we obtain

$$\frac{\partial Q}{\partial t} = -\gamma_p (Q - Q_o) \tag{A-84}$$

where we have replaced τ by t

and

$$Q_o = \rho_{co} + \rho_{vo} \tag{A-85}$$

Since it is assumed that a significant time will have elapsed between turning the device on and the beginning of optical amplification, Q will have reached its equilibrium value Q_o, and N will have an initial value equal to

$$N_{in} = \frac{\gamma_p - \gamma_s}{\gamma_p + \gamma_s} \rho_{co} - \rho_{vo} \tag{A-86}$$

For this reason, during the operating time, Eqs. (A-72) and (A-73) are identical and equal to

$$\frac{\partial N}{\partial t} = -(\gamma_p + \gamma_s)N + \gamma_p N_o - \gamma_s Q_o - \frac{\mu^2 \mathfrak{L}(\omega) |\mathscr{E}|^2 N}{\gamma_{cv} \hbar^2} \tag{A-87}$$

where $N_o = \rho_{co} - \rho_{vo}$. The population difference then has a formal solution given by

$$N(k,t,z) = \{N_{int} + (\gamma_p N_o - \gamma_s Q_o) \int_o^t dt' \exp[(\gamma_p + \gamma_s)t' + \frac{\mu^2 \mathfrak{L}(\omega)}{\gamma_{cv} \hbar^2} \int_o^{t'} |\mathscr{E}|^2 dt'']\}$$

$$\times \exp-[(\gamma_p + \gamma_s)t + \frac{\mu^2 \mathfrak{L}(\omega)}{\gamma_{cv} \hbar^2} \int_o^t |\mathscr{E}|^2 dt'] \tag{A-88}$$

Between pulses when the field is zero (since we have assumed that the polarization follows the field exactly), the population density will have a time dependence given by

$$N(k,t - t_o,z) = \left\{N_{int}(t_o) + \frac{(\gamma_p N_o - \gamma_s 0_o)}{\gamma_p + \gamma_s}[\exp(\gamma_p + \gamma_s)(t - t_o) - 1]\right\}$$

$$\times \exp -[(\gamma_p + \gamma_s)(t - t_o)] \qquad \text{(A-89)}$$

where Nint in Eq. (A-88) or $N_{int}(t_o)$ in Eq. (A-89) is the population difference at the beginning of a pulse. It could also be the difference just at the end of a pulse where the population again grows according to Eq. (A-89).

This allows one to determine the population density at the beginning of each pulse without having to perform integrations between pulses. If the complex field $\mathscr{E}$ is defined as

$$\mathscr{E}' = \mathscr{E}'\exp i\phi \qquad \text{(A-90)}$$

then Eqs. (A-70) and (A-71) are rewritten as

$$\frac{\partial \mathscr{E}'}{\partial z} = -L\mathscr{E}' - \frac{\eta\mu^2\mathscr{E}'}{2\hbar n_o^2\varepsilon_o}\int \frac{k^2 dk\ N(k,t,z)}{\gamma_{cv} + i(\nu - \omega)} \qquad \text{(A-91)}$$

For pulsed operation, Eq. (A-91) is solved for the real and imaginary parts given the results of Eq. (A-88) for N(k,t,z). The numerical procedures used to solve Eq. (A-91) differed considerably from the technique used for the steady-state case. A high-order Runge Kutta was used to perform the z integration. A straightforward trapezoidal rule was used to perform the time integrations in Eq. (A-88). The momentum integration was performed by assuming a polynomial fit to the third order in the k dependence of N(k,t,z). This third-order polynomial was then integrated analytically. The steps in the process involved are that at each z step a set of values for the

electromagnetic field at all given values of time for some previous z value are prescribed. These values of $\mathscr{E}$ are then used to determine the population difference at the given values of time and momentum. The integral over momentum is performed and the new set of $\mathscr{E}$ values are determined. Numerical results will be given after a discussion of device considerations.

6. DEVICE CONSIDERATIONS

In this report, we have used various values for the band-gap energy, electron mass in the different bands, and Fermi levels. In Section 2 and Fig. A-2, a specific model of a three-layer P-n-N device was given. The choice of this specific model was based on parameters for aluminum concentration and doping levels for devices grown during the experimental investigation, which were carried out concurrently with this work. The steps taken to obtain the various parameters given are taken from Ref. A-1, Chapter 4.

First, the band-gap energies for the direct, L, and X bands were determined for both the wide- and narrow-gap materials. Next, the electron and hole masses were determined for the conduction and valence bands. Both band-gap energy and mass are functions of aluminum concentration. The jumps in conduction and valence band energies were taken as 0.85 and 0.15 of the difference in direct band-gap energies. The Fermi levels were then determined from expressions relating the electron and hole carrier concentrations to the temperature, carrier mass, band-gap energies, and Fermi level. Assuming constant temperature, the Fermi levels can be determined by graphical solution. In the intrinsic region, a similar procedure gives the location of the Fermi level, though for this region the exponential approximation to the Fermi integrals may be used. The built-in fields and potentials are determined from Poisson's equation--one for each region. It is assumed that the mobile carriers can be neglected in the space charge region. By making use of the continuity of electric flux density and potential, we can express the potential in each region of the P-n-N device in terms of the built-in potential, the widths of the depletion region, the dielectric constants, and the charge densities. It is assumed that the entire intrinsic region is a space-charge

region. By using the continuity of the electric flux density at the junction of the n-N region, we can relate the depletion widths in the P and N regions.

Finally, using the equality of the total built-in potential and the sum of the built-in potential in each region, we can determine the depletion width in the N region by solving a quadratic equation. The total built-in potential is 1.836 eV, which in our case is the difference between the wide-gap direct band-gap energy and the sum of the Fermi-level energies of 0.085 and 0.064 eV (Eq. 4.3-8, Ref. A-1). It turns out that the device looks almost like a capacitor with most of the voltage drop across the intrinsic region (1.798 eV). The built-in potential on the P side is 0.0193 eV and on the N side is 0.0191 eV, whereas the corresponding depletion widths are 4.986 and 4.961 μm, respectively. With these numbers and the equations for the potentials, Fig. A-2(A) was drawn. If the device is biased by 1.836 V, then the band structure looks like Fig. A-2(B). It is assumed that this is the usual operating condition. The assumptions leading to the band structure in Fig. A-2(A) do not hold exactly for the completely biased case in Fig. A-2(B), because the intrinsic region is not an exactly uniform depletion region.

LABORATORY OPERATIONS

The Laboratory Operations of The Aerospace Corporation is conducting experimental and theoretical investigations necessary for the evaluation and application of scientific advances to new military space systems. Versatility and flexibility have been developed to a high degree by the laboratory personnel in dealing with the many problems encountered in the nation's rapidly developing space systems. Expertise in the latest scientific developments is vital to the accomplishment of tasks related to these problems. The laboratories that contribute to this research are:

Aerophysics Laboratory: Launch vehicle and reentry aerodynamics and heat transfer, propulsion chemistry and fluid mechanics, structural mechanics, flight dynamics; high-temperature thermomechanics, gas kinetics and radiation; research in environmental chemistry and contamination; cw and pulsed chemical laser development including chemical kinetics, spectroscopy, optical resonators and beam pointing, atmospheric propagation, laser effects and countermeasures.

Chemistry and Physics Laboratory: Atmospheric chemical reactions, atmospheric optics, light scattering, state-specific chemical reactions and radiation transport in rocket plumes, applied laser spectroscopy, laser chemistry, battery electrochemistry, space vacuum and radiation effects on materials, lubrication and surface phenomena, thermionic emission, photosensitive materials and detectors, atomic frequency standards, and bioenvironmental research and monitoring.

Electronics Research Laboratory: Microelectronics, GaAs low-noise and power devices, semiconductor lasers, electromagnetic and optical propagation phenomena, quantum electronics, laser communications, lidar, and electro-optics; communication sciences, applied electronics, semiconductor crystal and device physics, radiometric imaging; millimeter-wave and microwave technology.

Information Sciences Research Office: Program verification, program translation, performance-sensitive system design, distributed architectures for spaceborne computers, fault-tolerant computer systems, artificial intelligence, and microelectronics applications.

Materials Sciences Laboratory: Development of new materials: metal matrix composites, polymers, and new forms of carbon; component failure analysis and reliability; fracture mechanics and stress corrosion; evaluation of materials in space environment; materials performance in space transportation systems; analysis of systems vulnerability and survivability in enemy-induced environments.

Space Sciences Laboratory: Atmospheric and ionospheric physics, radiation from the atmosphere, density and composition of the upper atmosphere, aurorae and airglow; magnetospheric physics, cosmic rays, generation and propagation of plasma waves in the magnetosphere; solar physics, infrared astronomy; the effects of nuclear explosions, magnetic storms, and solar activity on the earth's atmosphere, ionosphere, and magnetosphere; the effects of optical, electromagnetic, and particulate radiations in space on space systems.


FILME
4
-84